Supplementary Information (SI) for Green Chemistry.
This journal is © The Royal Society of Chemistry 2026

Supporting Information

Accessing Photocatalytically Active Covalent Triazine-based Frameworks by Ball Milling: A Fast and Facile Synthesis Method

Leonie S. Häser[a], Sven Moos[a,b], Felix Egger[c], Keanu Birkelbach[d], Mirijam Zobel[c], Thomas Wiegand[a,b], Regina Palkovits*[a,b,d]

a. Institute of Technical and Macromolecular Chemistry (ITMC), RWTH Aachen University, Worringerweg 2, 52074 Aachen (Germany), E-mail: palkovits@itmc.rwth-aachen.de

b. Max Planck Institute for Chemical Energy Conversion, Stiftstr. 34-36, 45470 Mülheim an der Ruhr (Germany).

c. Institute of Crystallography, RWTH Aachen University, Jägerstraße 17-19, 52066 Aachen (Germany)

d. Forschungszentrum Jülich GmbH, Institute for Sustainable Hydrogen Economy (IHE-2), An der Deutschen Welle 7a, 52428 Jülich (Germany)

Content

S1. Materials

Terephthalimidamide dihydrochloride (BLD Pharm, 97 %), 1,4-benzendimethanol (abcr, 99 %), terephthalaldehyde (J&K, 99 %), cesium carbonate (Roth, ≥ 99.9 %), sodium chloride (Sigma-Aldrich, ≥ 99.0 %), potassium carbonate (abcr, 99 %), hydrochloric acid (ChemSolute, ≥ 37.0 %), and ethanol (technical grade) were used as purchased. Dimethyl sulfoxide (Thermo Scientific, ≥ 99.7 %) and tetrahydrofuran (ChemSolute, ≥ 99.9 %) applied in the reactions were degassed for 30 min prior to usage in addition to being handled under inert conditions. For the mechanochemical synthesis, a mini-mill Pulverisette 23 by Fritsch GmbH was used, equipped with a 15 mL stainless steel jar and one 15 mm stainless steel ball.

S2. General CTF Synthesis

All CTFs synthesized in this work were used at a particle size of < 200 µm after grinding in an agate mortar and sieving. All CTF yields were calculated using a theoretical molar mass based on the repeating unit of the CTF (128.15 g mol^{-1}).

S2.1. Solution-based

The synthesis of the solution-based CTF was performed, as previously reported, according to a modified literature procedure.[1,2]

Terephthalimidamide dihydrochloride (0.705 g, 3 mmol, 2 eq), 1,4-benzendimethanol (0.207 g, 1.5 mmol, 1 eq), and Cs_2CO_3 (2.156 g, 6.6 mmol, 4.4 eq) were dispersed in dry dimethyl sulfoxide (38 mL). The resulting suspension was heated to 100 °C. After 24 h, the temperature was increased to 160 °C for an additional 36 h. The resulting solid was filtered off and washed with 1 M $HCl_{(aq)}$, H_2O, EtOH, and THF (3x 19 mL each). The product was then dried under high vacuum, crushed in an agate mortar, and sieved (200 µm) to obtain a fine yellow powder (Yield: 0.563 g, 97.5 %).

S2.2. Mechanochemical

Terephthalimidamide dihydrochloride (0.705 g, 3 mmol, 2 eq), terephthalaldehyde (0.201 g, 1.5 mmol. 1 eq), and the respective basic salt additive (4.5 mmol, 3 eq) were added to the milling jar. The mixture was milled for different times at 50 Hz. Within this time, the jar was cooled down to room temperature and opened after 2 h, and 4 h of total milling time. The resulting mixture was washed out with 10 mL distilled water and EtOH each, stirred in distilled water (80 mL) for 30 min, before being washed with EtOH (20 mL) in the last purification step. The powder was then dried under high vacuum, crushed in an agate mortar, and sieved (200 µm) to obtain a fine yellow powder.

Table S1. Synthesis parameters and resulting yields for the bmCTFs discussed in this work.

Material	Milling Time	Base Additive		NaCl	Yield
10 min-bmCTF	10 min	Cs_2CO_3	1.470 g	-	0.305 g
20 min-bmCTF[a]	20 min	Cs_2CO_3	1.470	-	0.336 g
40 min-bmCTF	40 min	Cs_2CO_3	1.470	-	0.330 g, 57 %
1 h-bmCTF	1 h	Cs_2CO_3	1.470	-	0.391 g, 68 %
3 h-bmCTF	3 h	Cs_2CO_3	1.470	-	0.427 g, 74 %
5 h-bmCTF / C-bmCTF	5 h	Cs_2CO_3	1.470	-	0.468 g, 81 %
K-bmCTF	5 h	K_2CO_3	0.622 g	-	0.454 g, 79 %
KN-bmCTF	5 h	K_2CO_3	0.622 g	0.622 g	0.399 g, 69 %
P-bmCTF	5 h	Na_3PO_4	0.738	-	0.484 g, 83 %

[a] After a milling time of 20 min the obtained CTF showed a high sensitivity towards light exposure over several days resulting in a color change. This effect was not observed for the other milling times.

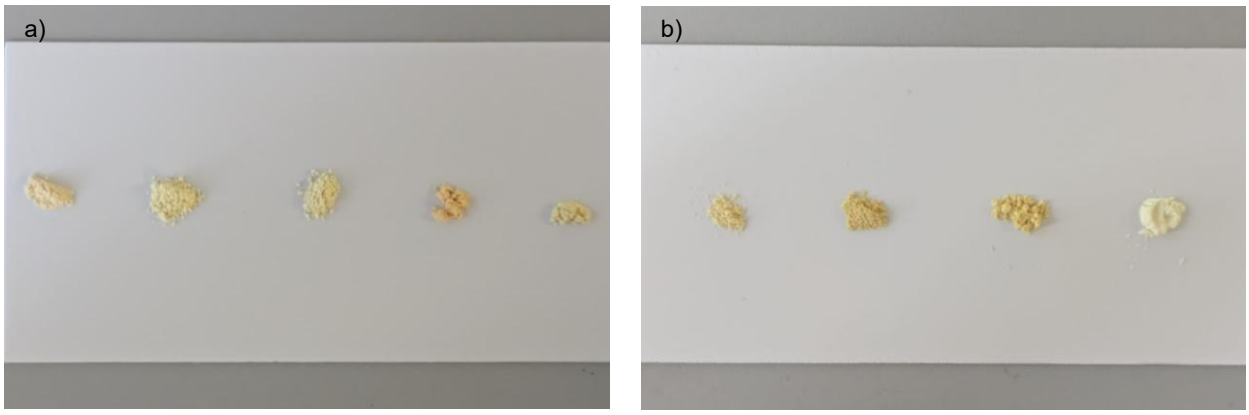

Figure S1. Photos of stCTF and the bmCTF synthesized at various times (a: left to right: 10 min, 20 min (different storages orders by decreasing light exclusion), 40 min; b: left to right: 1 h, 3 h, 5 h, stCTF).

S2.3. Synthesis of bmCTF$_x$

As a reference experiment, the equivalents of terephthalimidamide dihydrochloride applied in the synthesis were varied. The synthesis procedure, as well as the mass of terephthalaldehyde (0.201 g, 1.5 mmol. 1 eq) and Cs_2CO_3 (4.5 mmol, 3 eq), were kept constant for all variations. The amount of amidine applied and the mass of product are given in Table S2. As the assumed molar mass per polymer unit does not account for structural variation, no yield is calculated for this set of experiments.

Table S2. Monomer equivalents, amount of terephthalimidamide dihydrochloride used in the synthesis and product mass of the bmCTF$_x$.

Material	eq(aldehyde) : eq(amidine)	n(amidine)	Product mass
bmCTF$_1$	1 : 1	1.5 mmol	0.289 g
bmCTF$_{1.5}$	1 : 1.5	2.25 mmol	0.438 g
bmCTF$_2$ / 5 h-bmCTF	1 : 2	3 mmol	0.468 g
bmCTF$_3$	1 : 3	4.5 mmol	0.440 g

S2.4. Synthesis of stbmCTF

An 5 h-bmCTF (101.8mg), synthesized via the procedure described in section S2.2, and Cs_2CO_3 (209.6 mg) were suspended in dried DMSO (10 mL) under N_2-atmosphere. The mixture was heated to 160 °C for 24 h. The obtained solid was filtered off and washed analogously to the synthesis of the stCTF. The product was dried at 60 °C under reduced pressure, crushed in an agate mortar, and sieved (200 µm) to obtain a dark yellow powder (62.9 mg).

S2.5. Comparison of Green Metrics

For both synthesis procedures, solvothermal and mechanochemical, energy input, environmental factor (E-factor) with and without water, as well as the process mass intensity (PMI) with and without water were calculated according to literature.[3] Both calculations were done as described in section S2.1 and S2.2.

Energy Input:
To estimate of energy input $\mathrm{E_{in}}$ needed for both reactions, the power consumption $\mathrm{E_{con}}$ of the heating plate and ball mill device were multiplied with the respective reaction time t. I should be noted, that this calculation gives a rough estimate about the order of magnitude.

$$\mathrm{E_{in}} = \mathrm{E_{con}} \cdot t$$

Process Mass Intensity (PMI):
As for the E-factors, the PMIs calculation was performed each with and without considering water consumption during purification.

$$\mathrm{PMI} = \frac{m_{\text{total mass used in process}}}{m_{\text{product}}}$$

Environmental Factor (E-factor):
The E-factors were calculated twice: considering water consumption during purification and without. Waste production due to non-reacted educts were considered based on the respective product yield. As expected, this assumption resulted in the correlation PMI = E-factor + 1.

$$\mathrm{E-factor} = \frac{m_{\text{wastes}}}{m_{\text{product}}}$$

S3. Characterization of the CTFs

S3.6. IR Spectroscopy

The following DRIFTS experiments were performed using a Bruker VERTEX 70 spectrometer equipped with a Harrick Scientific praying mantis with controllable atmosphere and heating unit. All experiments were performed in a wavenumber range of 800 – 4000 cm^{-1} using an MCT detector at a resolution of 1 cm^{-1}. All samples were degassed at 120°C for 20 min under nitrogen atmosphere prior to the IR experiments.

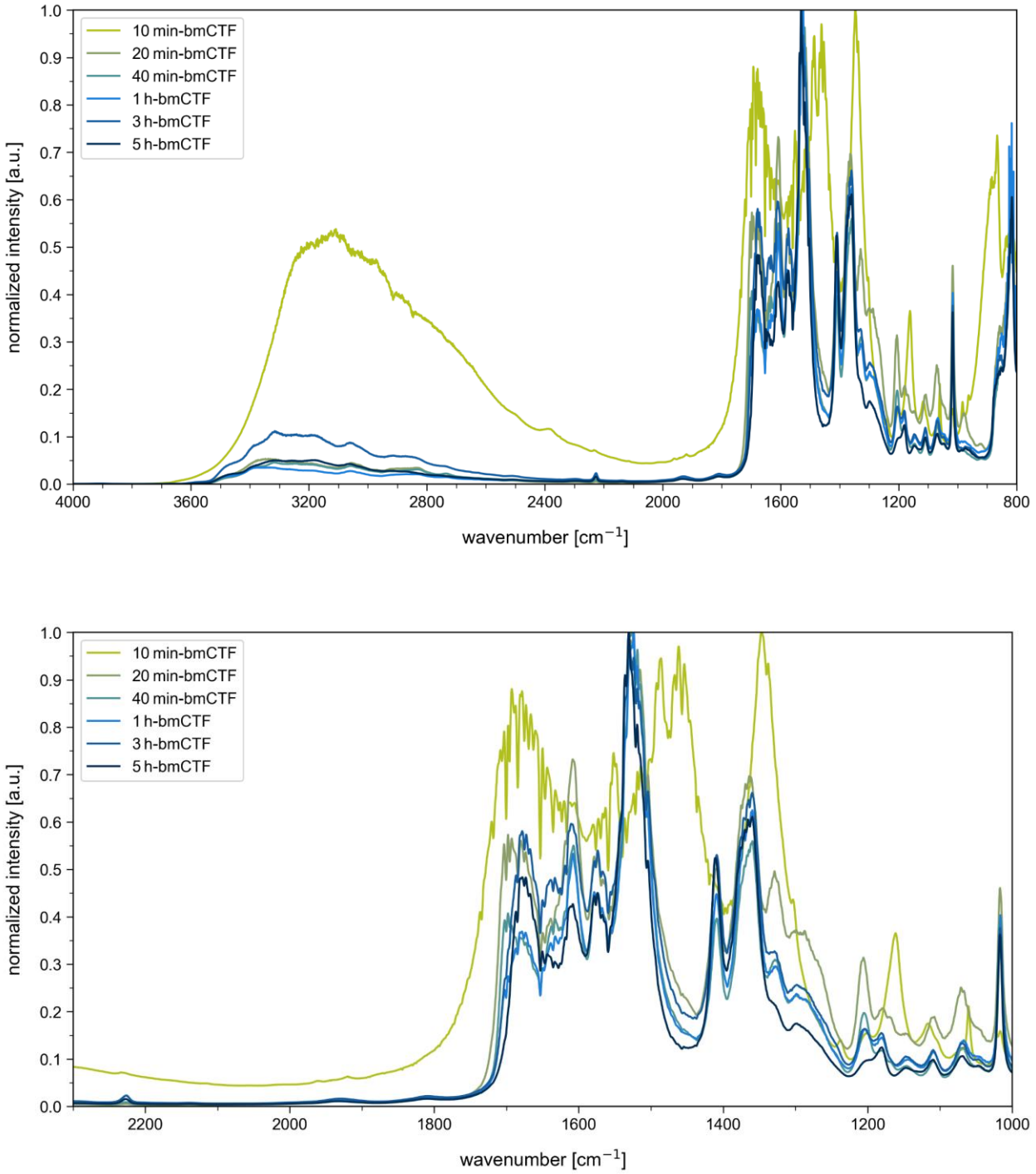

Figure S2. DRIFTS spectra for the bmCTFs at varying milling times of 10 min (pale green) to 5 h (dark blue). Top: whole FTIR spectrum, bottom: FTIR zoomed into the fingerprint region up to 2300 cm^{-1}.

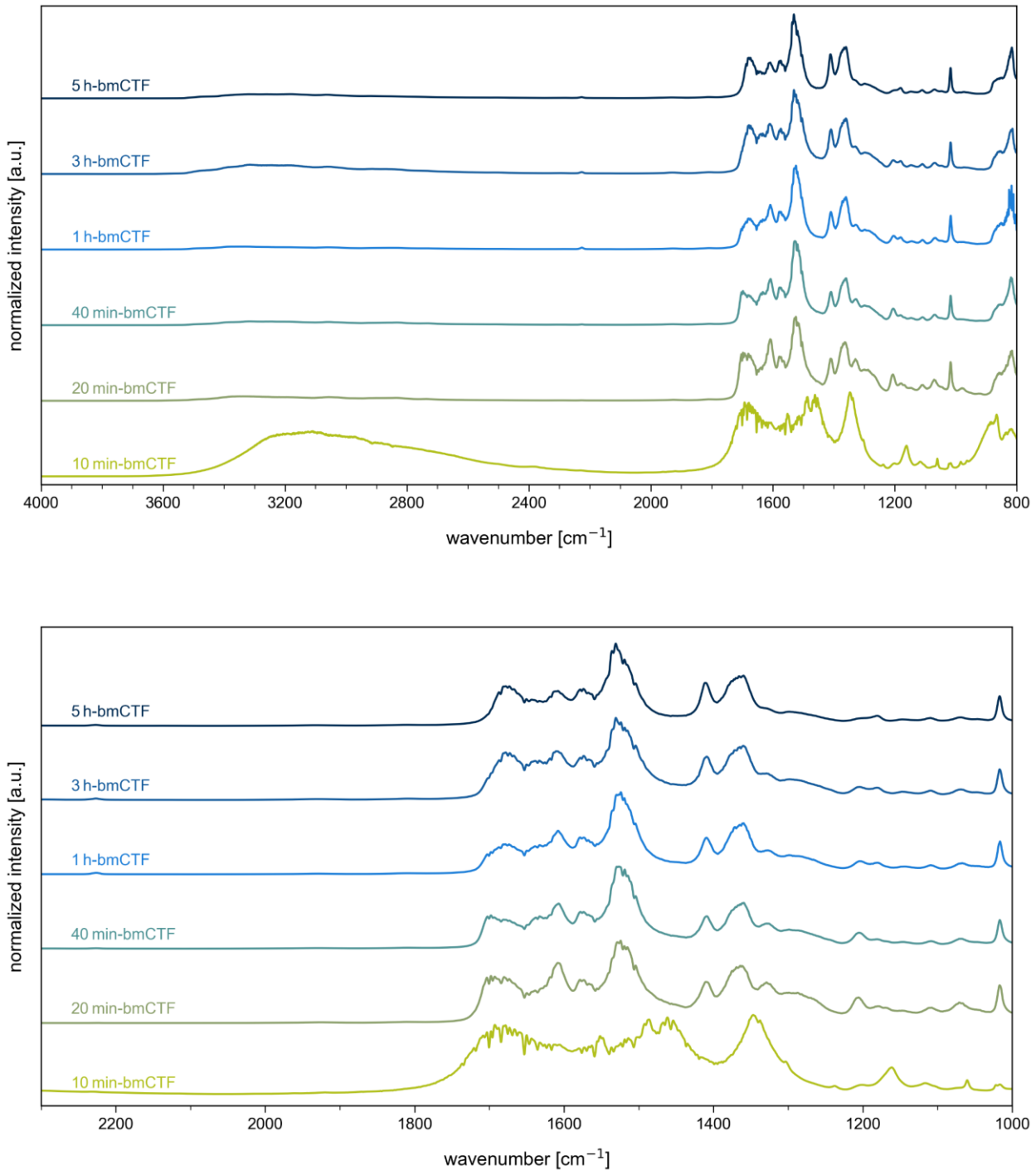

Figure S3. Stacked DRIFTS spectra for the bmCTFs at varying milling times of 10 min (pale green) to 5 h (dark blue). Top: whole FTIR spectrum, bottom: FTIR zoomed into the fingerprint region up to 2300 cm^{-1}.

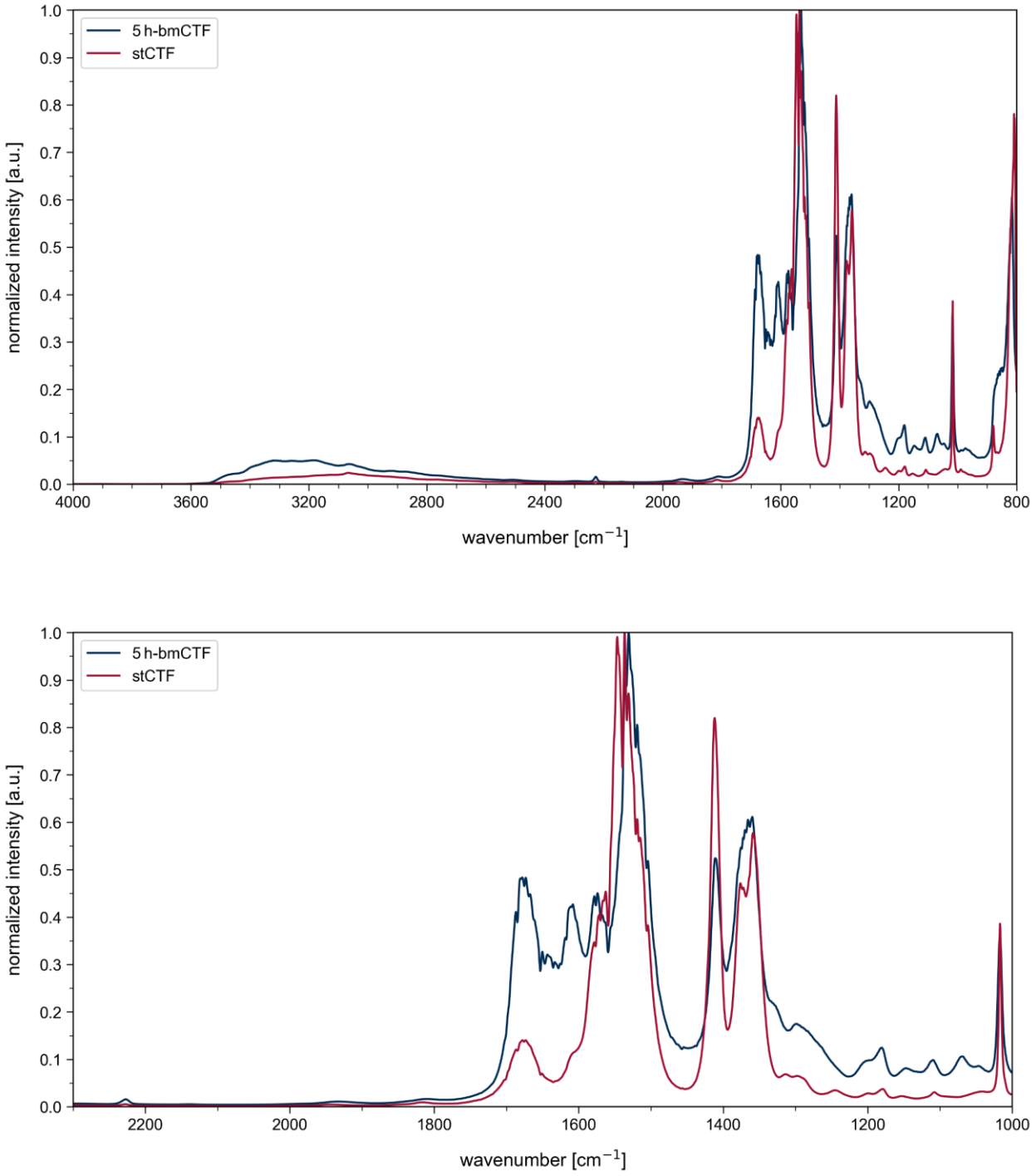

Figure S4. DRIFTS spectra for the 5h-bmCTF (blue), and stCTF (red). Top: whole FTIR spectrum, bottom: FTIR zoomed into the fingerprint region up to 2300 cm^{-1}.

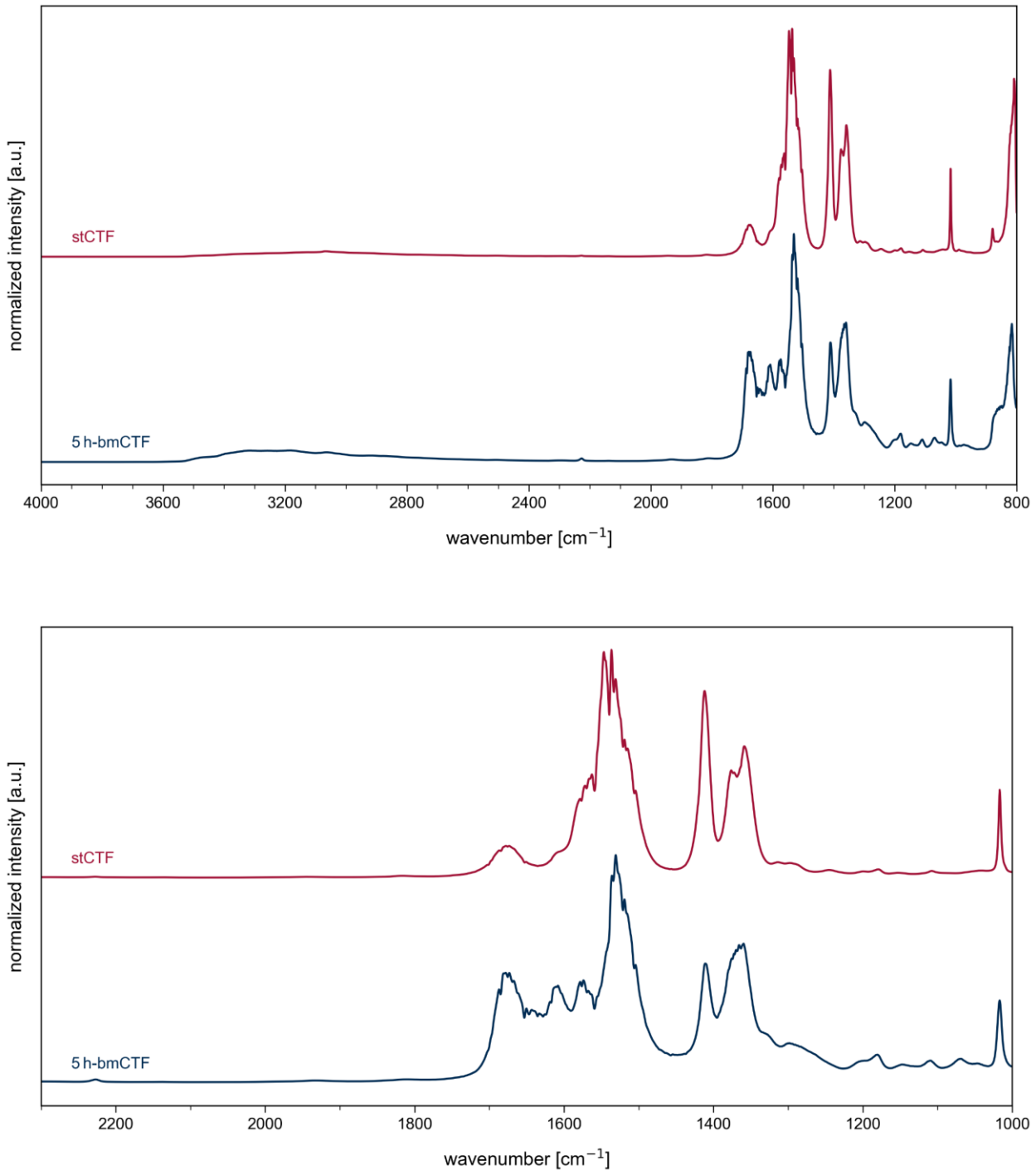

Figure S5. Stacked DRIFTS spectra for the 5h-bmCTF (blue), and stCTF (red). Top: whole FTIR spectrum, bottom: FTIR zoomed into the fingerprint region up to 2300 cm^{-1}.

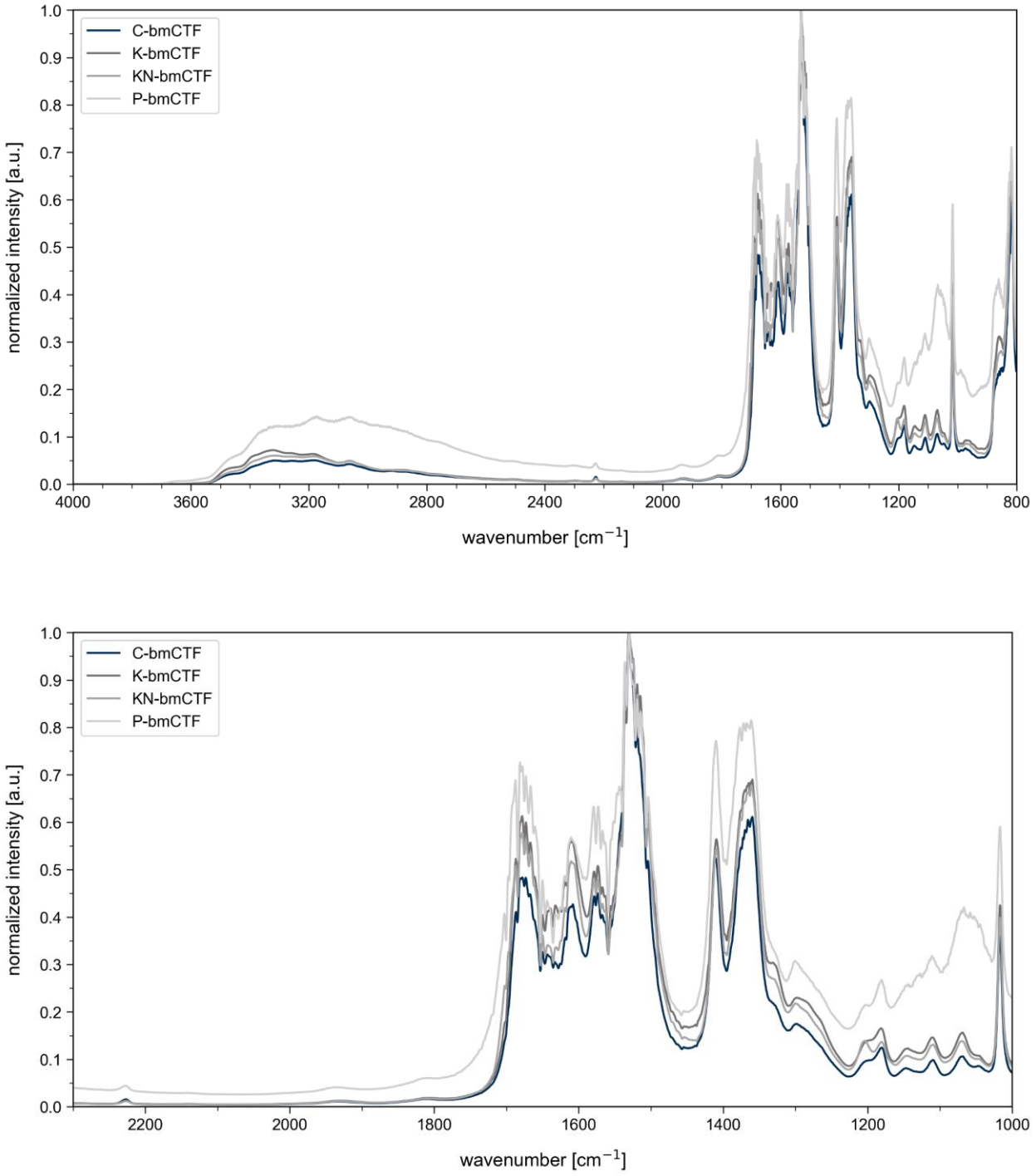

Figure S6. DRIFTS spectra for the C-bmCTF (blue), K-bmCTF (dark grey), KN-bmCTF (grey), and P-bmCTF (light grey). Top: whole FTIR spectrum, bottom: FTIR zoomed into the fingerprint region up to 2300 cm^{-1}.

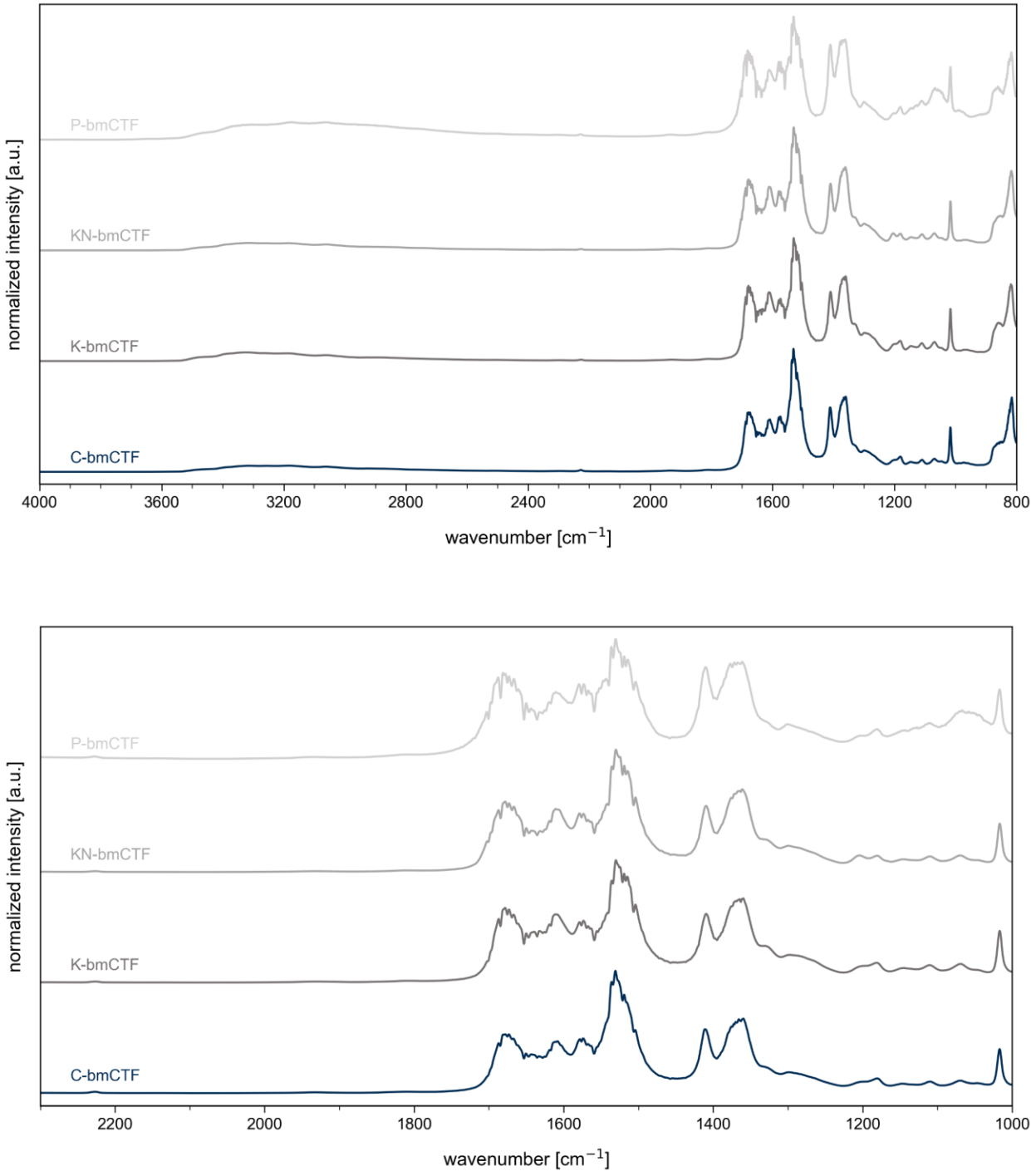

Figure S7. Stacked DRIFTS spectra for the C-bmCTF (blue), K-bmCTF (dark grey), KN-bmCTF (grey), and P-bmCTF (light grey). Top: whole FTIR spectrum, bottom: FTIR zoomed into the fingerprint region up to 2300 cm^{-1}.

The following DRIFTS spectra were recorded as described in the wavenumber range of 850 – 4000 cm^{-1}, with the exception that the samples were not degassed prior to measurement. All measurements were taken at room temperature against a KBr background.

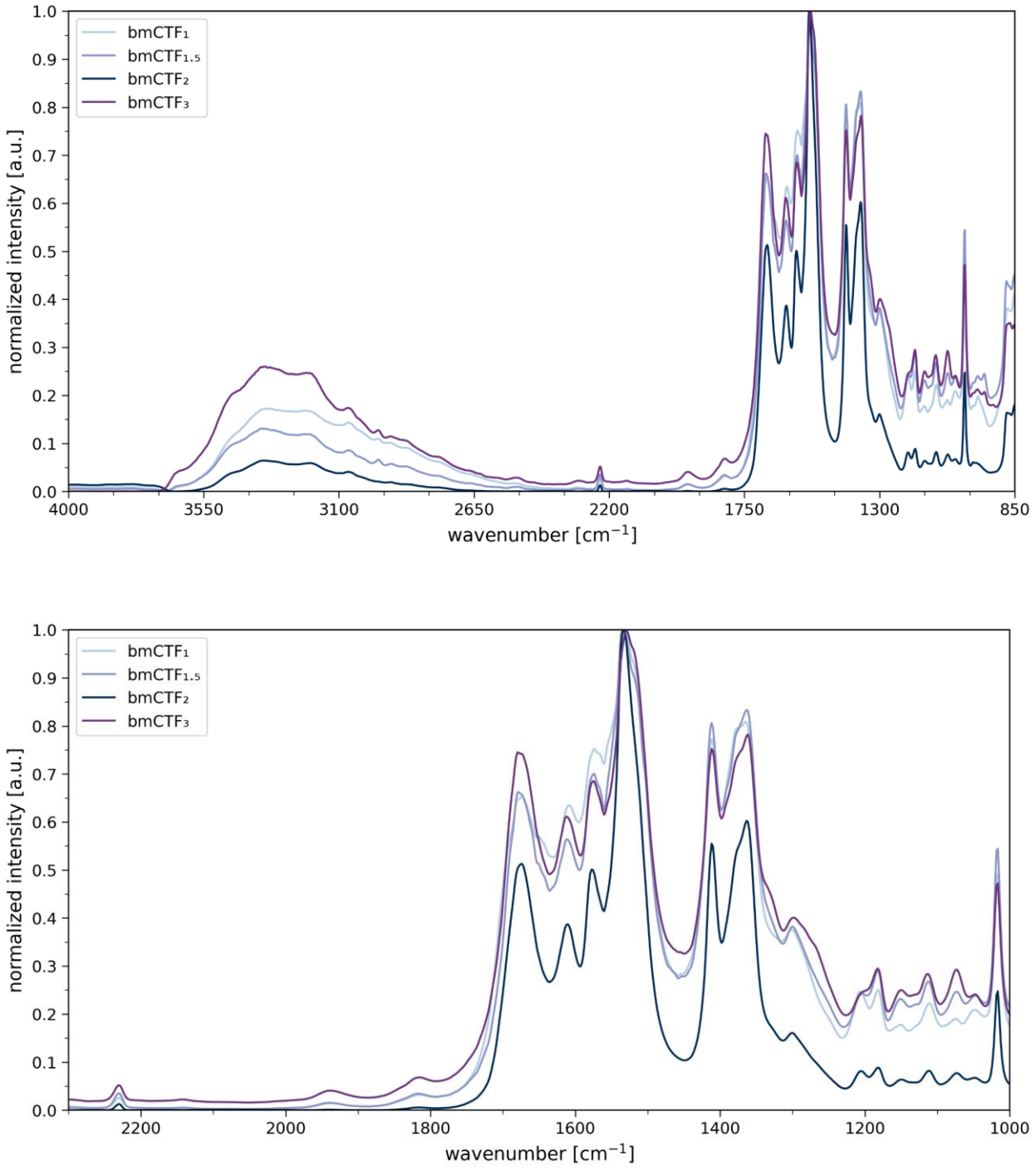

Figure S8. DRIFTS spectra for the $bmCTF_x$ spectra using various equivalents of the monomers (aldehyde : amidine, light blue to dark blue for increasing amidine content). Top: whole FTIR spectrum, bottom: FTIR zoomed into the fingerprint region up to 2300 cm^{-1}. All spectra were measured under atmospheric conditions and without heating prior to the measurement.

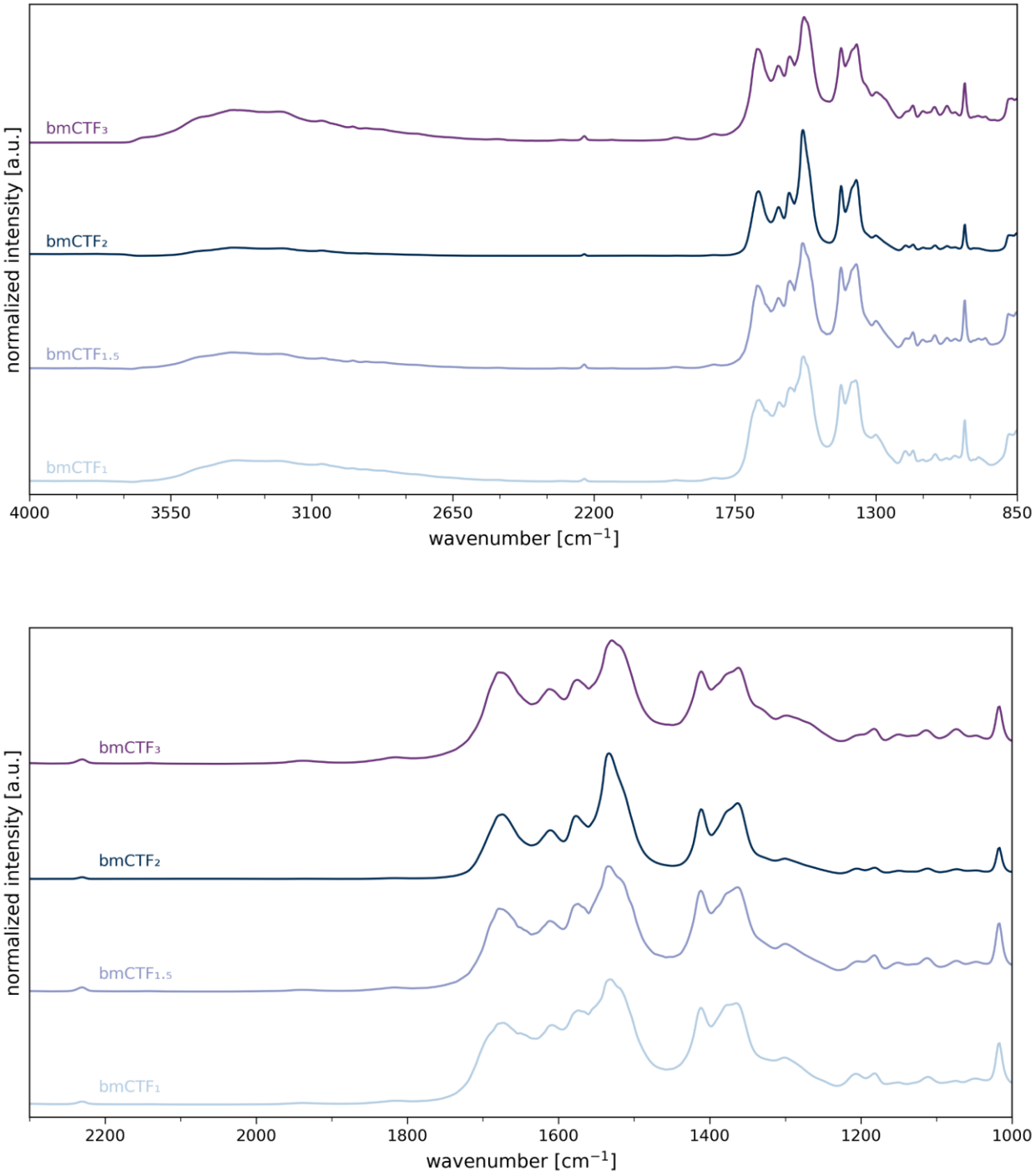

Figure S9. Stacked DRIFTS spectra for the $bmCTF_x$ spectra using various equivalents of the monomers (aldehyde : amidine, light blue to dark blue for increasing amidine content). Top: whole FTIR spectrum, bottom: FTIR zoomed into the fingerprint region up to 2300 cm^{-1}. All spectra were measured under atmospheric conditions and without heating prior to the measurement.

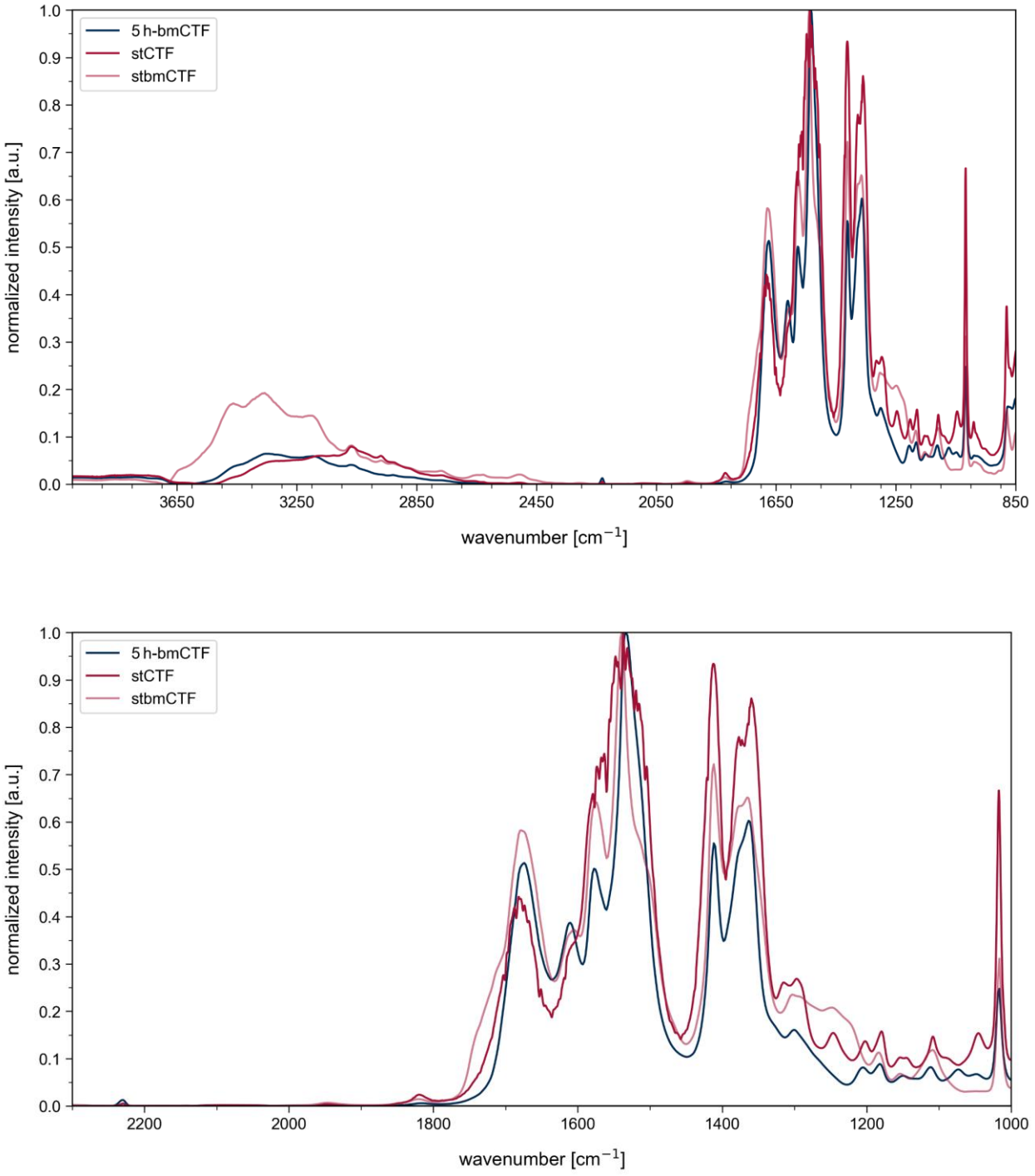

Figure S10. DRIFTS spectra for the 5 h-bmCTF (blue), stCTF (dark red) and stbmCTF (light red). Top: whole FTIR spectrum, bottom: FTIR zoomed into the fingerprint region up to 2300 cm^{-1}. All spectra were measured under atmospheric conditions and without heating prior to the measurement.

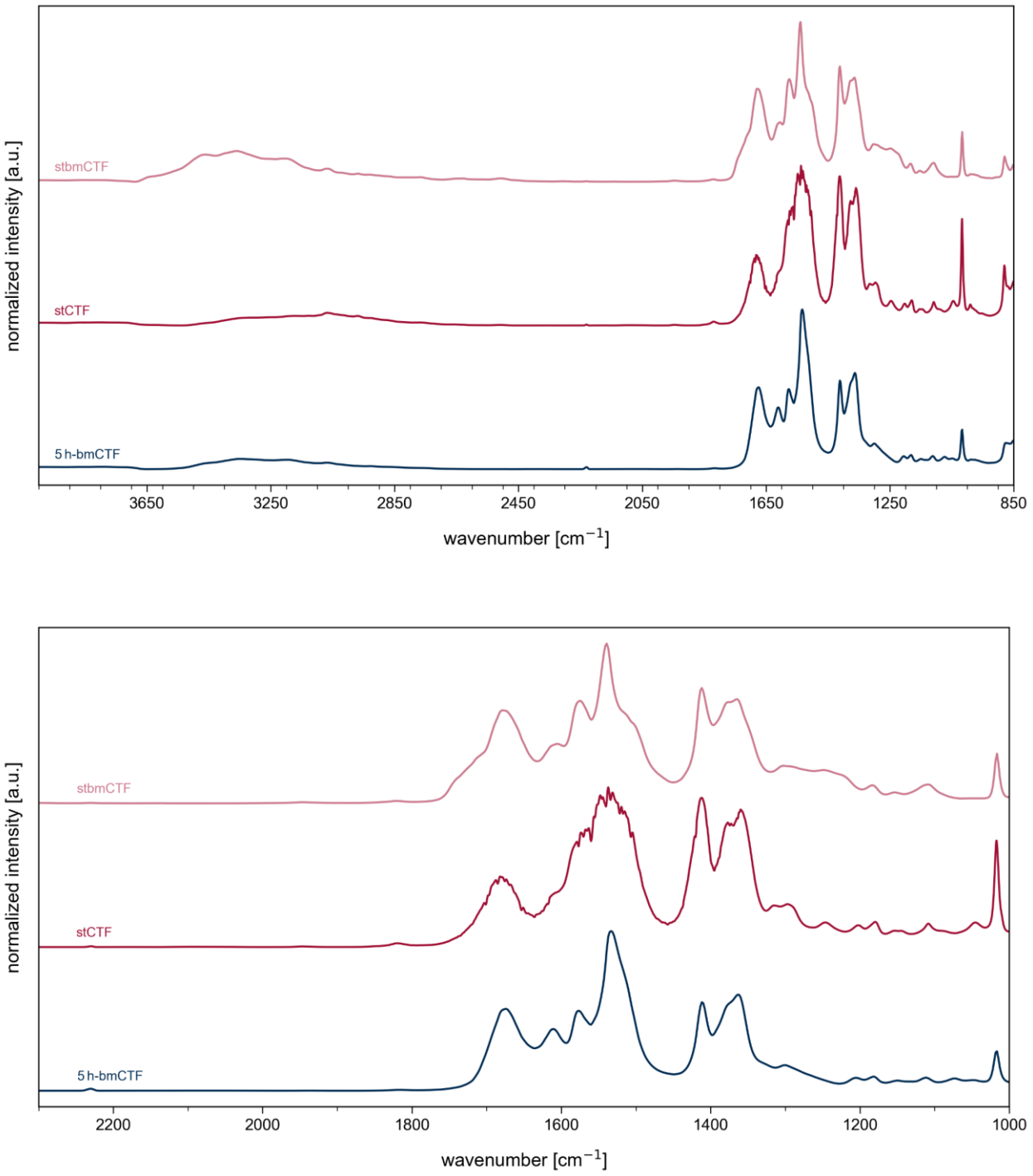

Figure S11. Stacked DRIFTS spectra for the 5 h-bmCTF (blue), stCTF (dark red) and stbmCTF (light red). Top: whole FTIR spectrum, bottom: FTIR zoomed into the fingerprint region up to 2300 cm^{-1}. All spectra were measured under atmospheric conditions and without heating prior to the measurement.

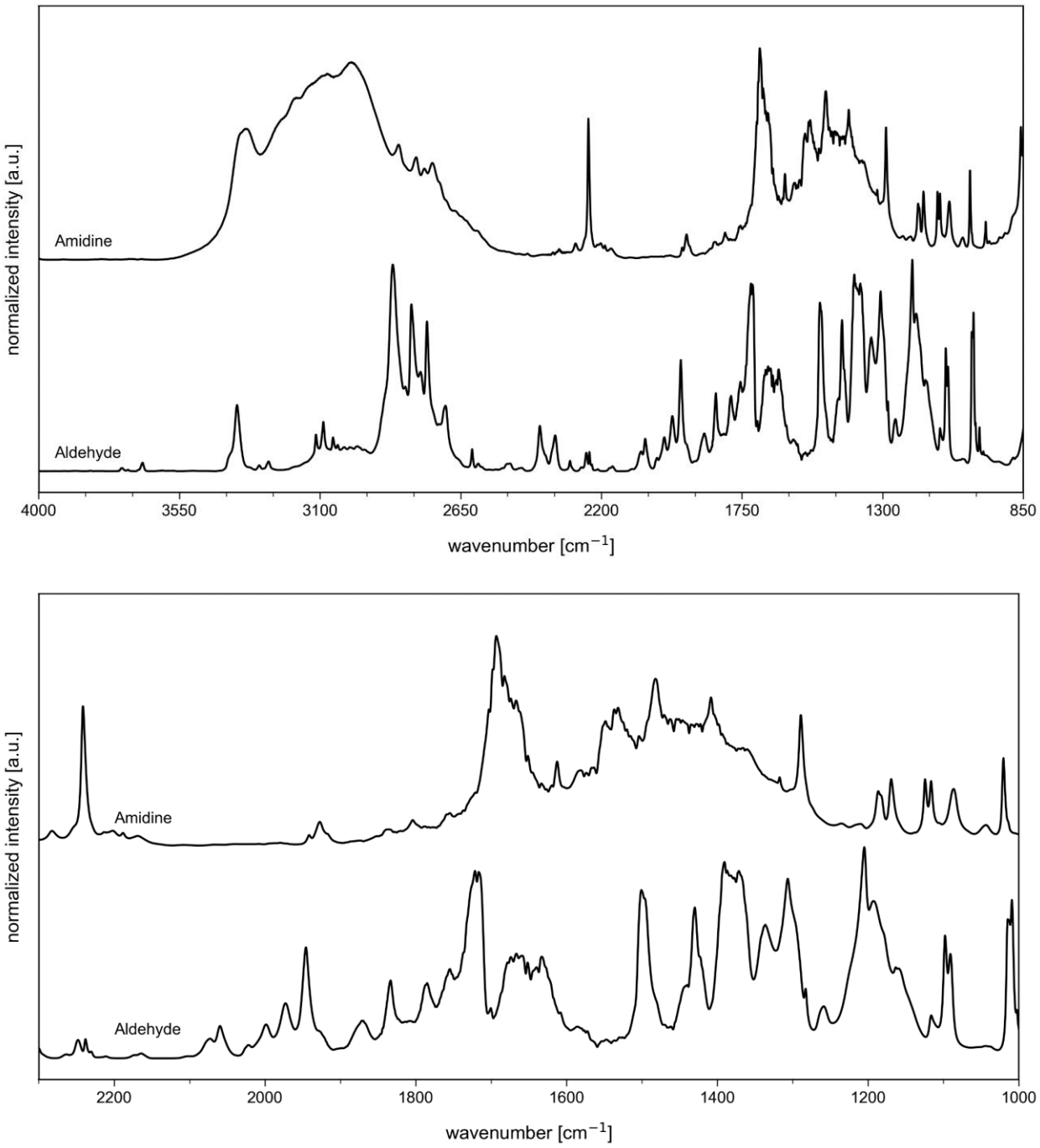

Figure S12. Stacked DRIFTS spectra for the monomers terephthalimidamide dihydrochloride **(1)** and terephthalaldehyde **(2)**. Top: whole FTIR spectrum, bottom: FTIR zoomed into the fingerprint region up to 2300 cm^{-1}.

S3.7. Solid-state NMR Spectroscopy

The solid-state NMR spectra were acquired at a magnetic-field strength of 16.4 T using a Bruker double-resonance 3.2 mm probe with a MAS frequency of 17.0 kHz. Experimental parameters were optimized directly on the measured sample. Data processing was conducted with the software Topspin (version 4.1.3). No line broadening (LB) was applied during processing unless otherwise stated. All spectra were normalized to the highest peak intensity. The temperature was maintained at 275 K (Bruker BCU temperature) using a Bruker BCU II unit. Spectra were referenced to TMS, with the methylene resonance of adamantane serving as a secondary standard. Exemplary experimental conditions are provided in Table S3.

Table S3. Exemplary conditions for the ^{1}H-^{13}C CP-MAS NMR measurements.

^{1}H-^{13}C CP-MAS Experiment	**ν_r = 17.0 kHz**	**ν_r = 20.0 kHz**
B_0 [T]	16.4	16.4
CP polarization Transfer	H-C CP	H-C CP
$\nu_1(^{1}H)$ [kHz]	60	80
$\nu_1(^{13}C)$ [kHz]	47	24
Shape	Tangent shape[4,5]	Tangent shape[4,5]
^{13}C carrier [ppm]	150	150
CP contact time [µs]	1000	1500
Sweep width [ppm]	568	568
Acquisition time [ms]	25.6	25.6
^{1}H Spinal64 decoupling [kHz]	90	78
Number of scans	512[a,b]	6144
Interscan delay [s]	10	10
Measurement time [min]	85	1026
Probe target temperature [K]	275	275

[a]for terephthalaldehyde 4096 scans and LB of 50 Hz were applied.

[b]for the long-term measurement 6144 scans were recorded.

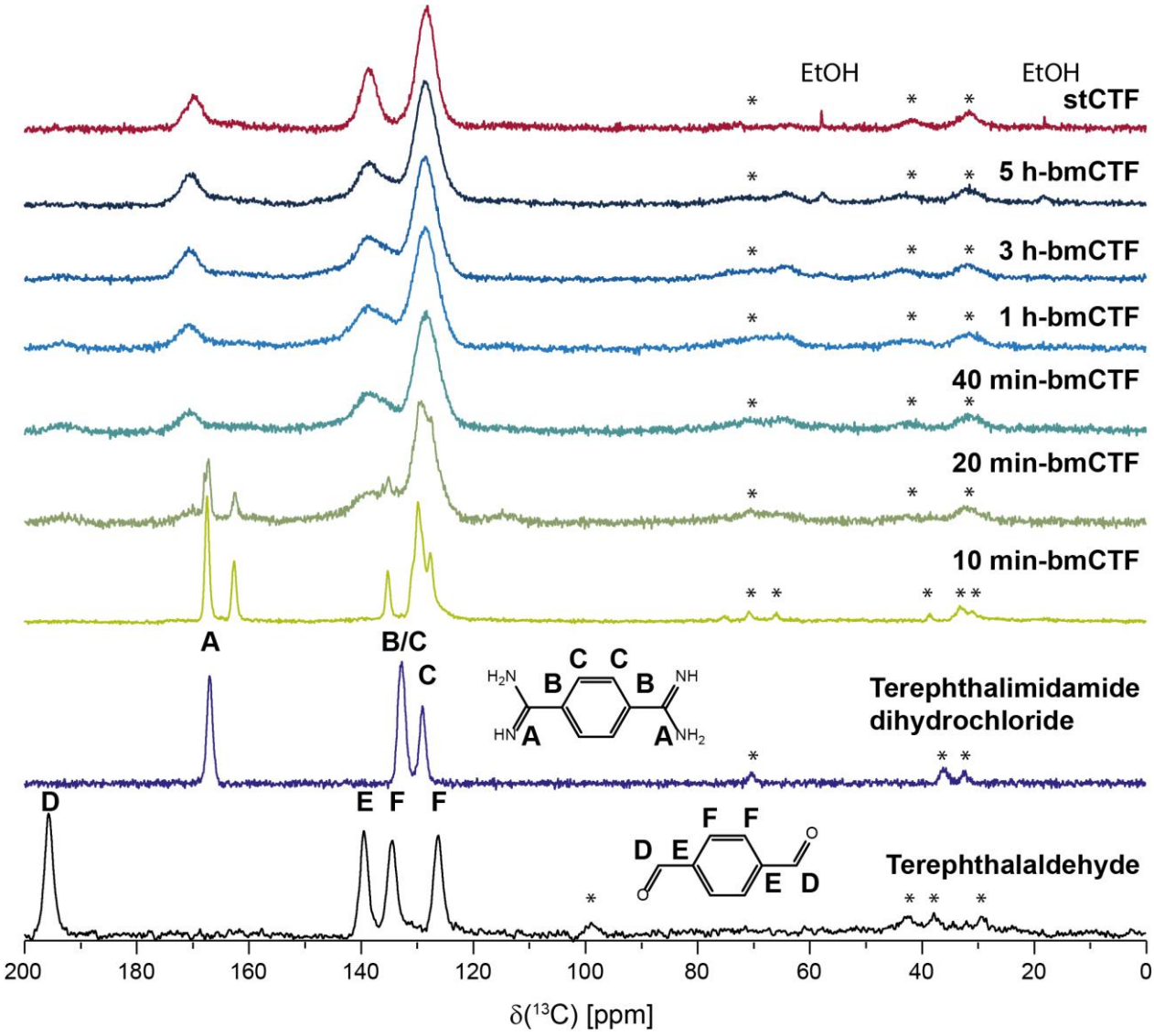

Figure S13. Stacked ^{1}H-^{13}C CP-MAS NMR spectra (recorded at 16.4 T and 17.0 kHz MAS frequency) of bmCTFs obtained for different milling times, as well as the stCTF and the reaction substrates (* indicate MAS sidebands). Sharp resonances around 20 and 60 ppm can be assigned to remaining ethanol residues from the washing procedure. The resonance assignment of the terephthalimidamide dihydrochloride spectrum is based on dipolar-dephasing ^{13}C NMR experiments (spectra not shown).

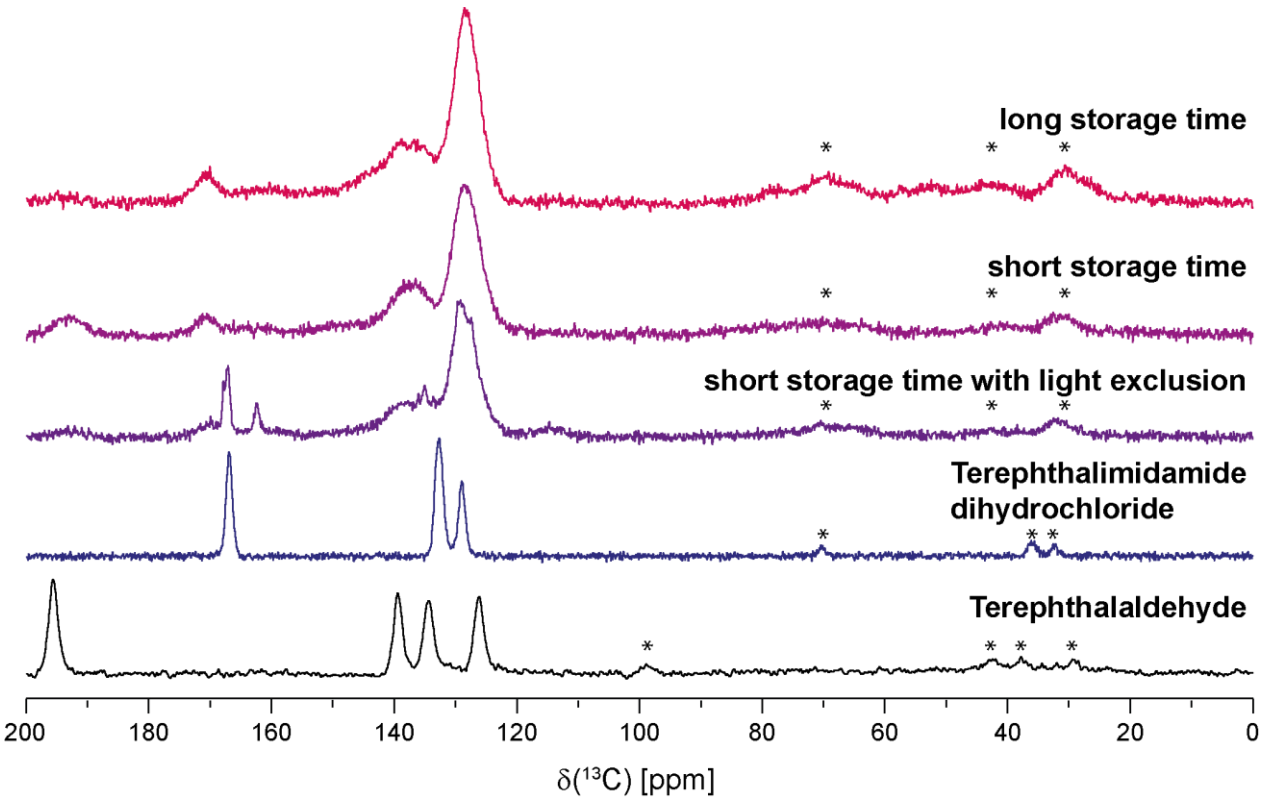

Figure S14. Stacked ^{1}H-^{13}C CP-MAS spectra (recorded at 16.4 T and 17.0 kHz MAS frequency) of terephthalimidamide dihydrochloride, terephthalaldehyde and three 20 min-bmCTF samples stored under different conditions (* indicate MAS sidebands).

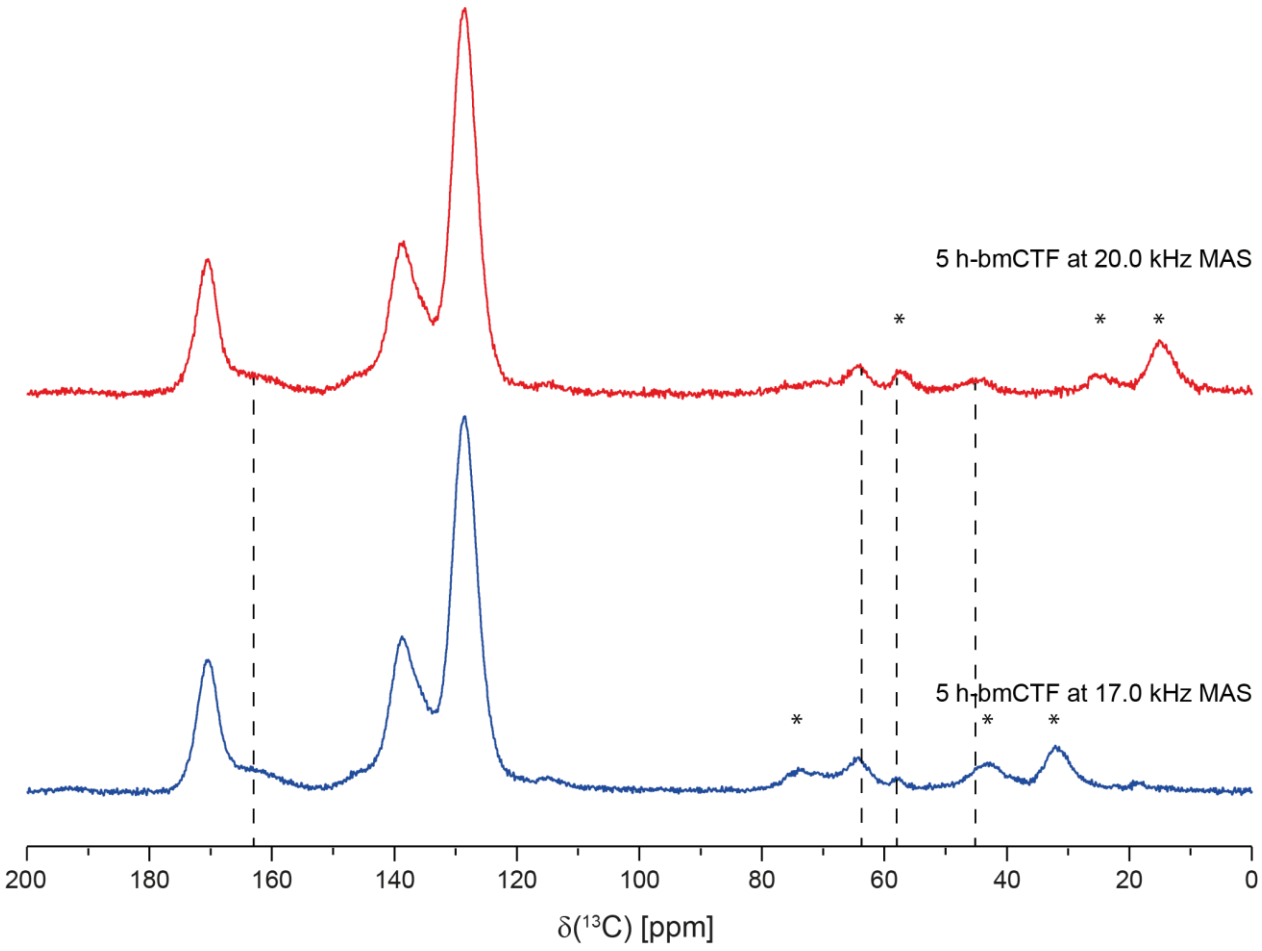

Figure S15. Stacked ^{1}H-^{13}C CP-MAS NMR spectra of the 5 h-bmCTF (recorded at 16.4 T and 6144 scans) measured with two different MAS frequencies of 17.0 and 20.0 kHz (* indicate MAS sidebands). Broad signals at around 162 ppm and in the region between 50-80 ppm could be identified pointing to a possible intermediate.

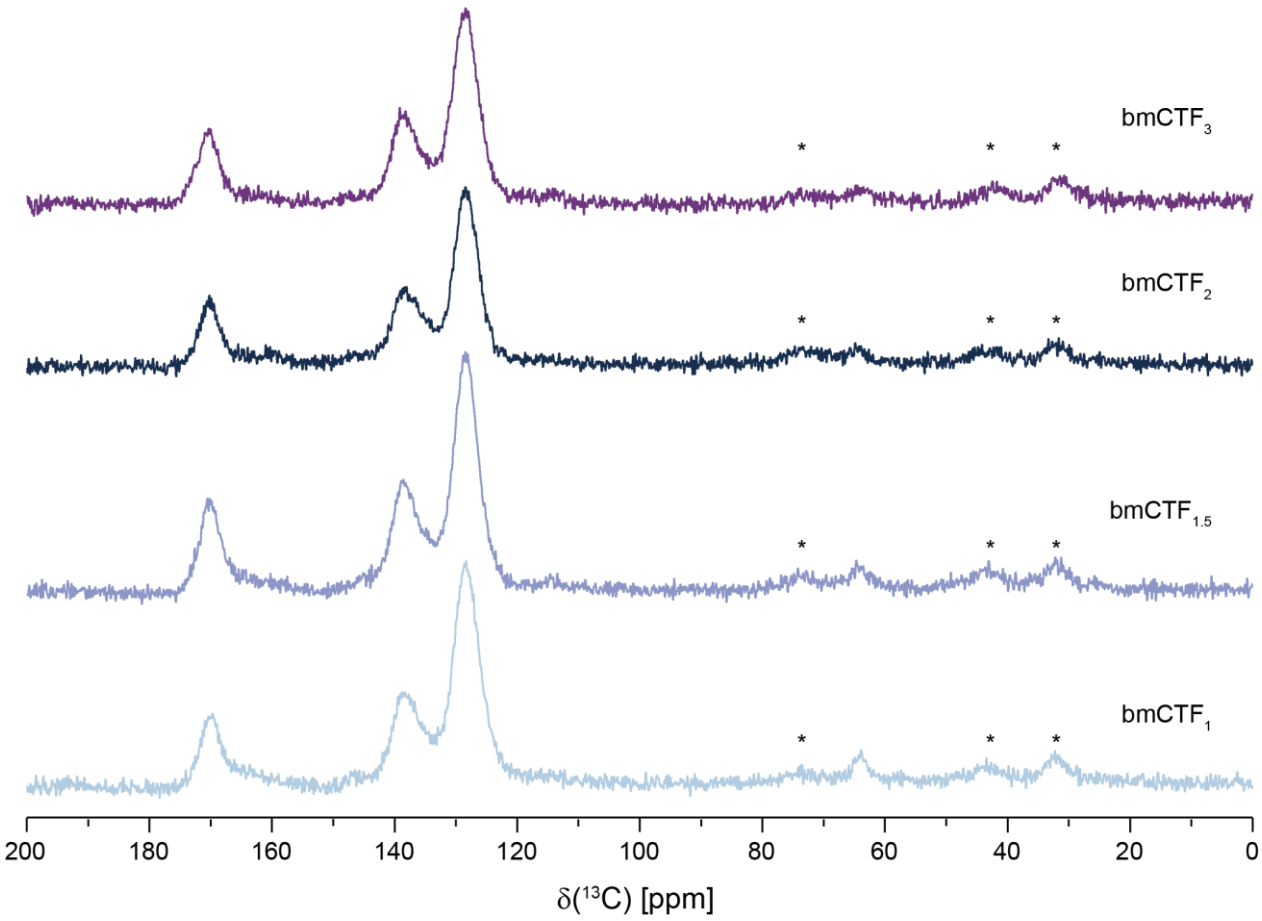

Figure S16. Stacked ^{1}H-^{13}C CP-MAS NMR spectra (recorded at 16.4 T and 17.0 kHz MAS frequency) of 5 h-bmCTF samples prepared with different substrate equivalents (* indicate MAS sidebands). In contrast to the IR spectra, no substrate resonances are detected as the applied measuring conditions favor the detection of CTF resonances over those of the aldehyde.

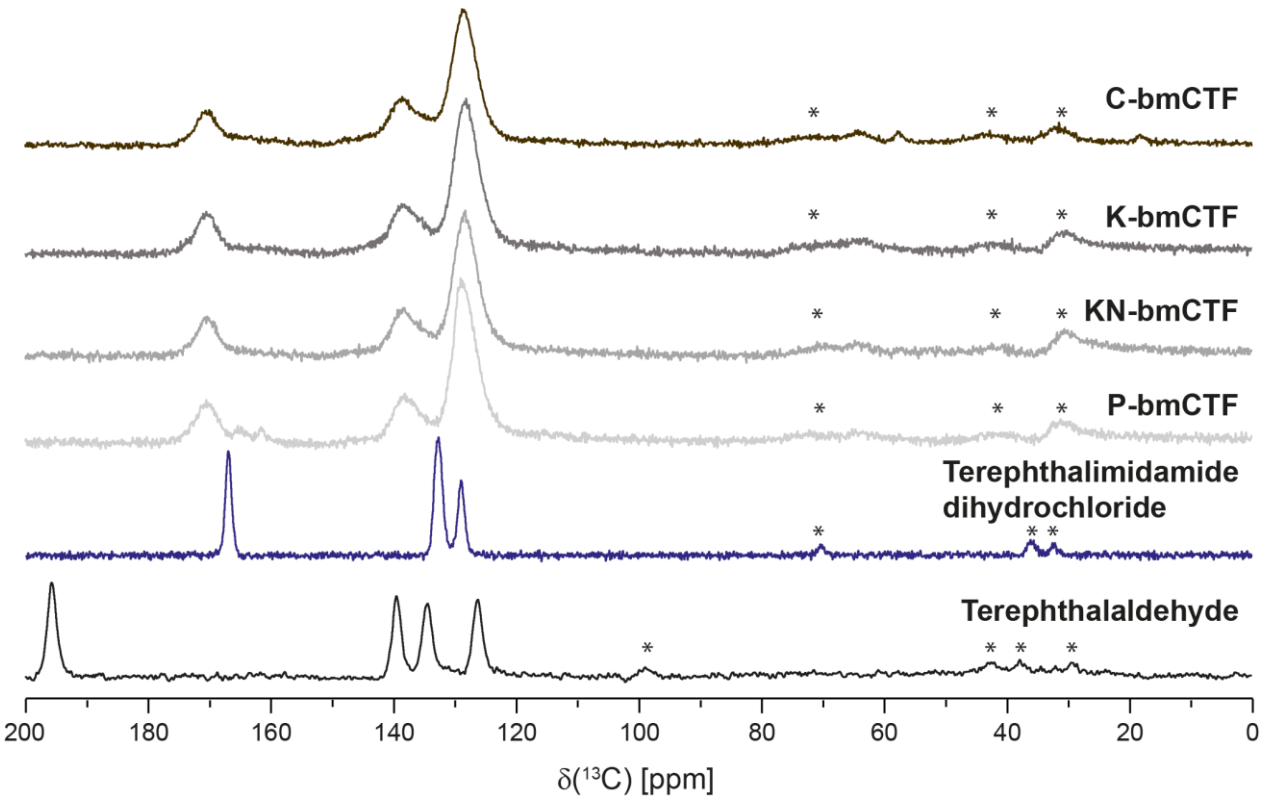

Figure S17. Stacked ^{1}H-^{13}C CP-MAS NMR spectra (recorded at 16.4 T and 17.0 kHz MAS frequency) of terephthalimidamide dihydrochloride, terephthalaldehyde and different additives used for the mechanochemical CTF synthesis (* indicate MAS sidebands).

S3.8. XRD and PDF

Powder X-ray total scattering data was acquired at Beamline I15-1 Diamond Light Source, using an energy of 76.67 keV (wavelength = 0.0162 nm) and a Perkin Elmer XRD 4343 CT detector. The powder sample was packed in borosilicate glass capillaries with an outer diameter of 2 mm (inner diameter 1.56 mm). Measurements were taken for 30 seconds and corrected for detector dark field, flat field and polarization prior to integration into Q using the DAWN software.[6] Figure S17 shows the diffraction patterns of the 5 h-bmCTF (blue) and the KN-bmCTF (dark grey) compared to the stCTF (red). The PXRD patterns consist mostly of a diffuse scattering component. As common XRD techniques are not suited for gaining structural insight of such amorphous materials, the pair distribution function (PDF) can help in structural characterization of the systems short range order.[7] The PDF technique, as it is obtained by the Fourier transformation of the total scattering pattern, utilizes not only the Bragg scattering, but also the diffuse scattering intensity, representing the structural information as a histogram of all interatomic distances in real space.[8] Corresponding PDFs have been generated based on the PXRD with a Q-range of 0.36 up to 18.2 $Å^{-1}$ using the PDFgetX3 software and are shown in Fig. S18.[9] They have been corrected for scattering contributions of the borosilicate glass capillaries, as well as for atomic form factors, polarization, self-absorption, multiple scattering and Compton scattering.

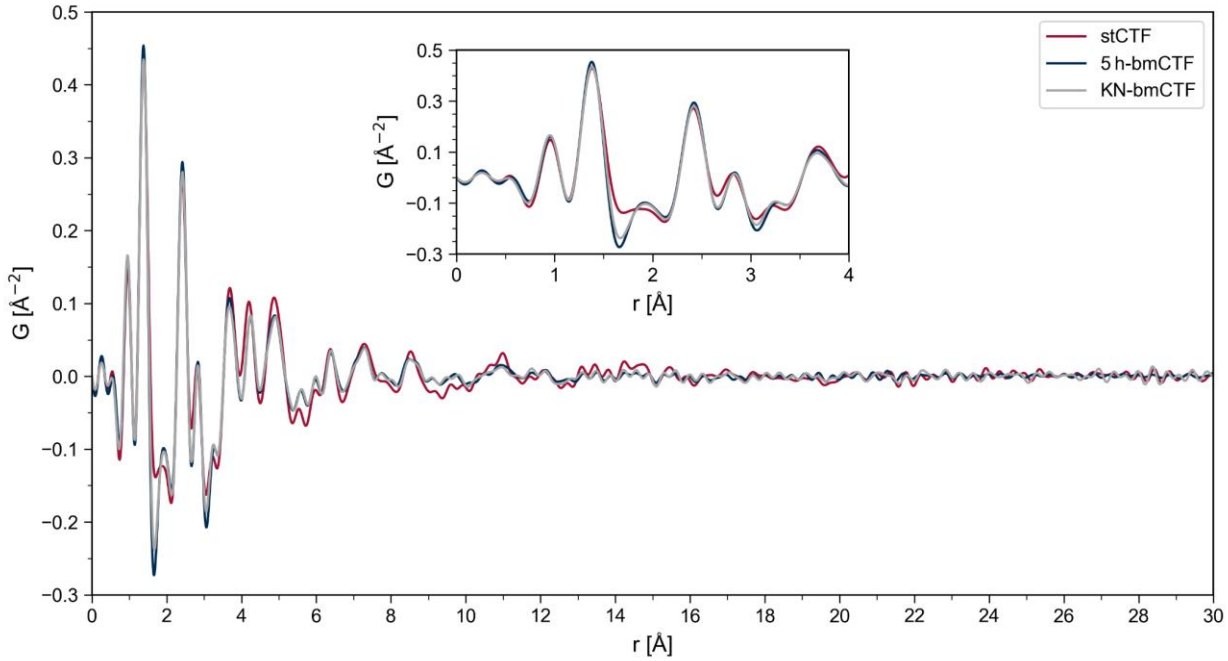

Figure S18. Pair Distribution Function (PDF) plots derived from the total scattering data for 5h-bmCTF / C-bmCTF (blue), KN-bmCTF (dark grey), and stCTF (red) samples. The PDFs reveal the short-range order in the predominantly amorphous materials, which seem to show no sign of any long-range stacking order.

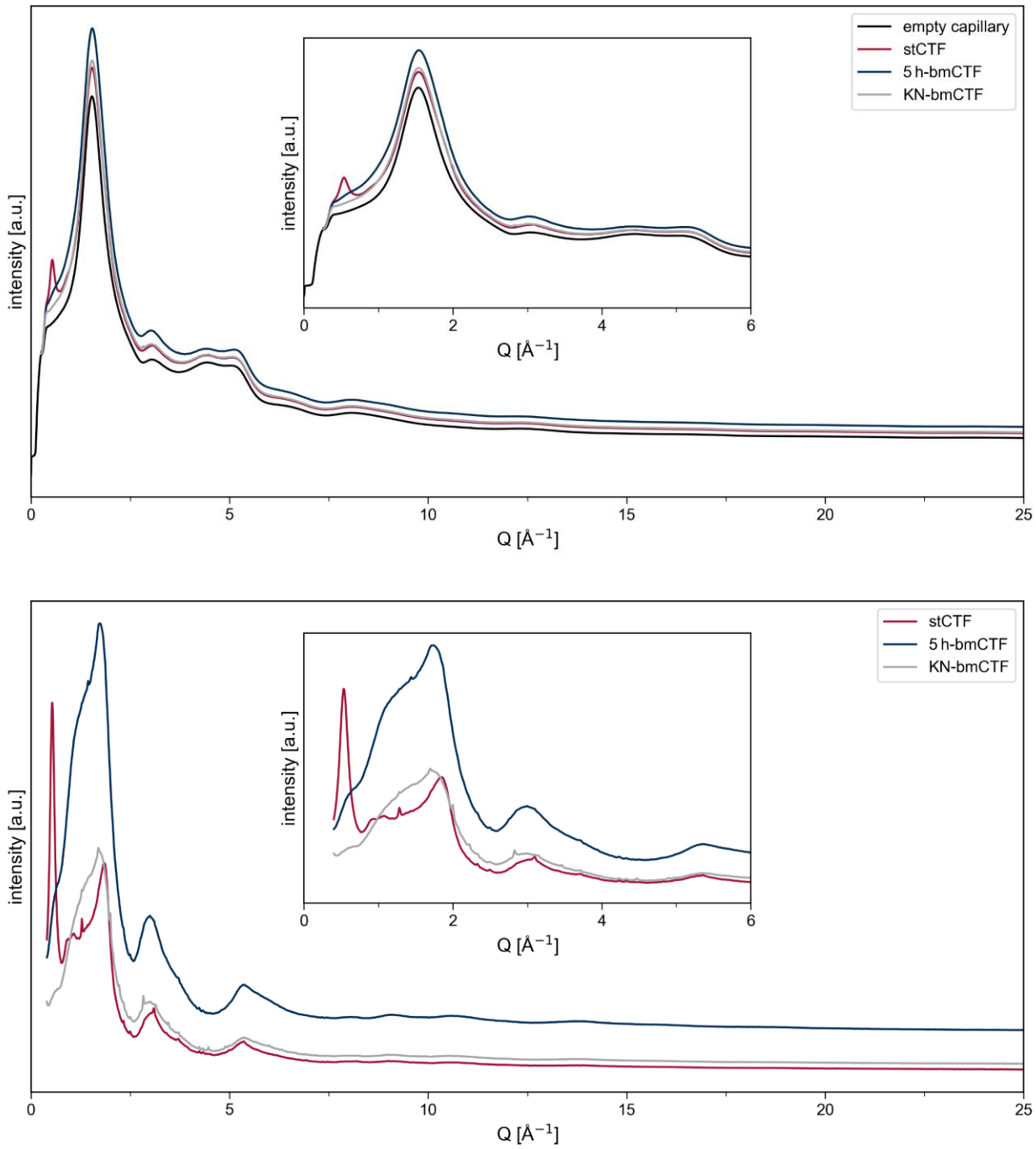

Figure S19. PXRD data of the of the 5 h-bmCTF / C-bmCTF (blue), the KN-bmCTF (dark grey) and stCTF (red) before (upper figure) and after subtraction (lower figure) of the empty capillary (dashed line). Data is plotted in Intensity (y-axis) vs scattering vector Q, also known as the magnitude of the momentum transfer of the scattered x-rays given with $Q = 4\pi \sin\theta / \lambda$.

The following powder X-ray diffraction (PXRD) patterns were recorded using a Bruker D2 Phaser Diffractometer equipped with a Cu Kα source. The experiments were conducted at 30 kV and 10 mA, collecting the data in the 2 θ range of 6 ° to 90 °for a total measuring time of 60 min.

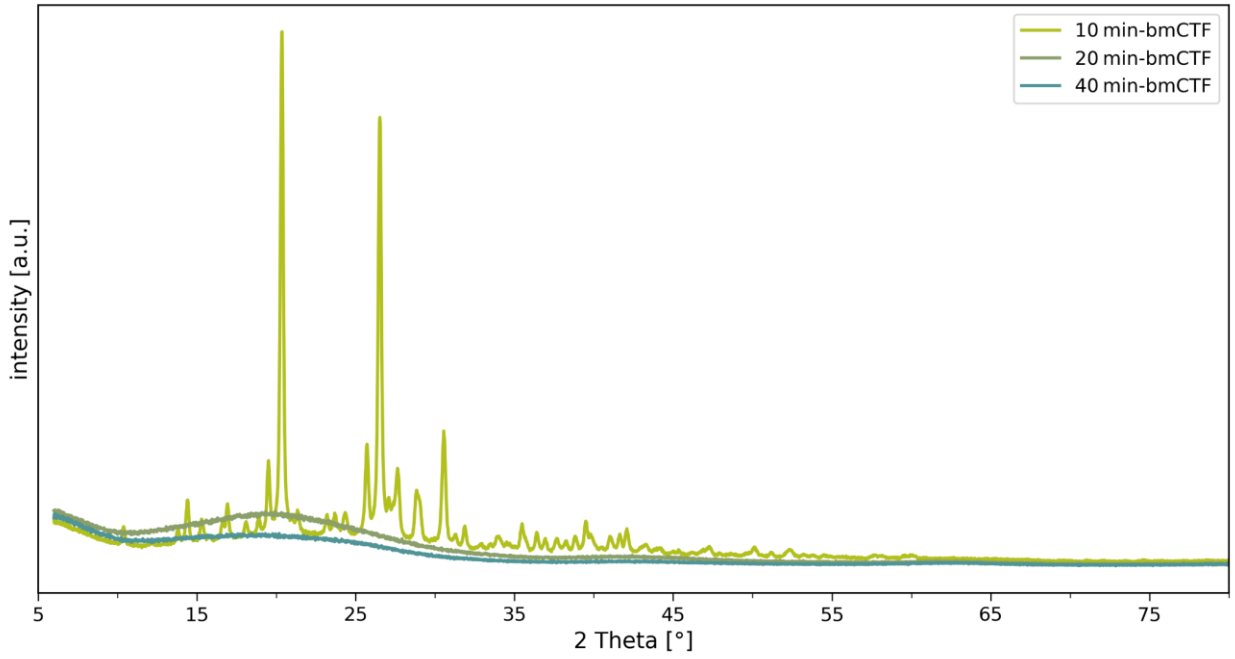

Figure S20. PXRD pattern of the bmCTFs milled for less than one hour (light to dark green with longer milling time).

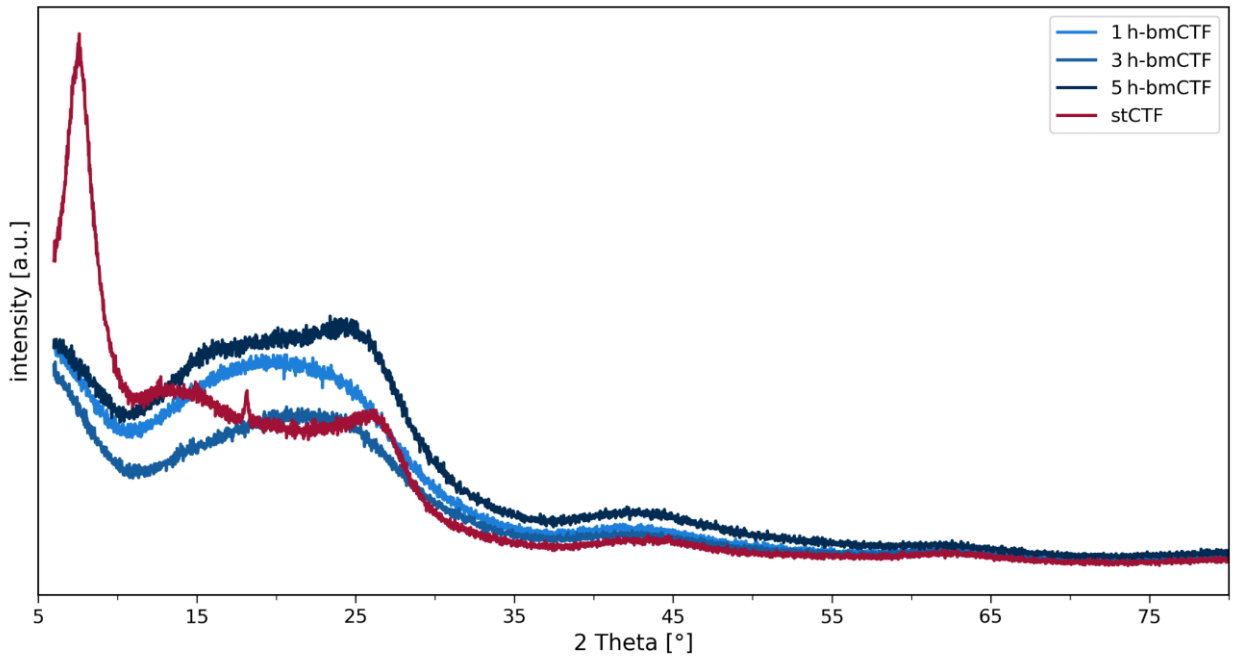

Figure S21. PXRD pattern of the bmCTFs milled for one hour ad longer (light to dark blue with longer milling time), as well as the stCTF (red).

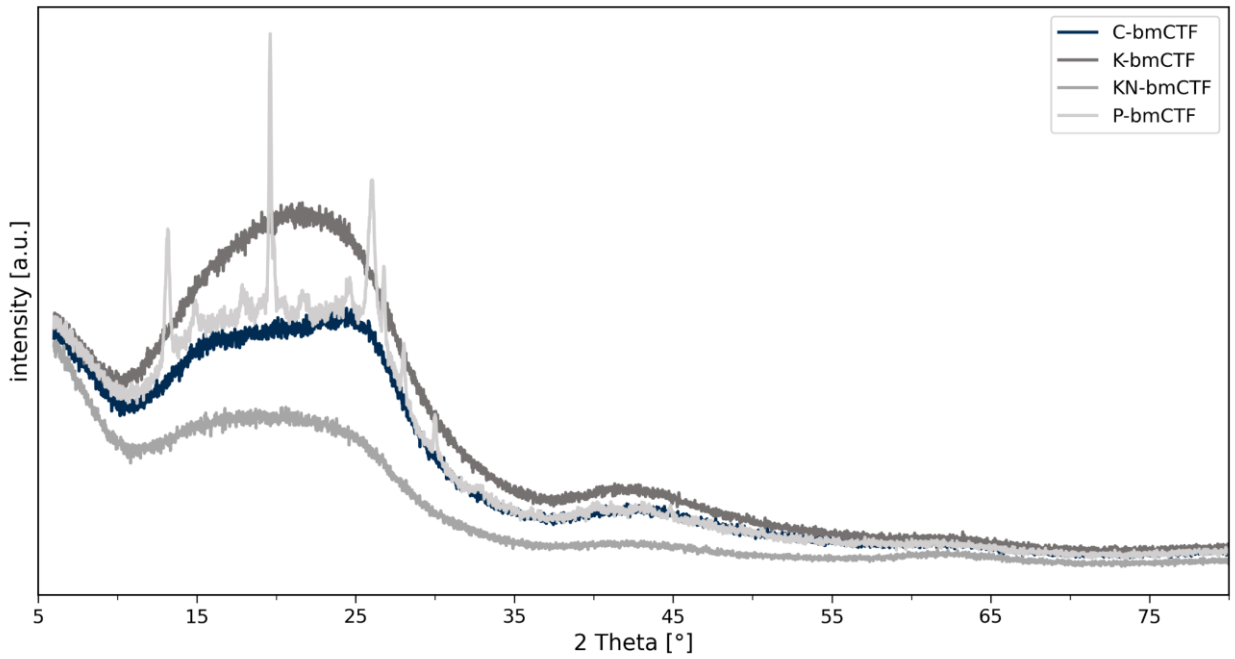

Figure S22. PXRD pattern of the of the bmCTFs synthesized using varying salt additive: C-bmCTF (blue), K-bmCTF (dark grey), KN-bmCTF (grey), and P-bmCTF (light grey).

S3.9. ICP and Elemental Analysis

Inductively coupled plasma (ICP) spectroscopy for cesium, iron and chromium, as well as and elemental analysis were performed by Mikroanalytisches Laboratorium Kolbe.

Table S4. Elemental Analysis and ICP for the stCTF and 5 h-bmCTF compared to theoretical values for an ideal framework.

Material	C [%]	H [%]	N [%]	Cs [ppm]	Fe [%]	Cr [%]
Theoretical	74.99	3.15	21.86	-	-	-
stCTF	63.86	4.66	17.43	62	0.23	0.05
5 h-bmCTF	63.53	4.98	17.71	39	0.20	0.03

S3.10. N_2-Pysisorption

Physisorption experiments were conducted at an ASAP 2060 Analyzer by Micromeritics using N_2 adsorptive gas and cooling the samples to 77 K. Prior to the physisorption experiments, all samples were degassed at 150 °C. The obtained data was evaluated using the MicroActive software by applying the BET model for surface area evaluation. The total pore volume was obtained from the adsorbed gas volume at a relative pressure of p/p_0.

Table S5. N_2-physisoprtion for the CTFs synthesized in this work.[a]

Material	Surface Area [$m^2\ g^{-1}$]	External Surface Area [$m^2\ g^{-1}$]	Total Pore Volume [$cm^3\ g^{-1}$]	Micropore Volume [$cm^3\ g^{-1}$]
stCTF	592	222	0.201	0.192
20 min-bmCTF	110	104	0.304	0.002
40 min-bmCTF	72	66	0.151	0.003
1 h-bmCTF	30	27	0.046	0.001
3 h-bmCTF	27	26	0.062	0.001
5 h-bmCTF / C-bmCTF	32	31	0.064	0.000
K-bmCTF	29	26	0.062	0.001
KN-bmCTF	51	48	0.129	0.001
P-bmCTF	31	30	0.065	0.000

[a]Due to the low thermal stability no comparable data could be obtained for the 10 min-bmCTF.

S3.11. Water-Physisorption

Water adsorption measurements were conducted at 20 °C using an Autosorb iQ instrument by 3P Instruments. 20 – 30 mg of sample were degassed for 3 h prior to analysis. Adsorption was performed within a relative pressure range of 0.053–0.09, followed by desorption between 0.90 and 0.05 relative pressure.

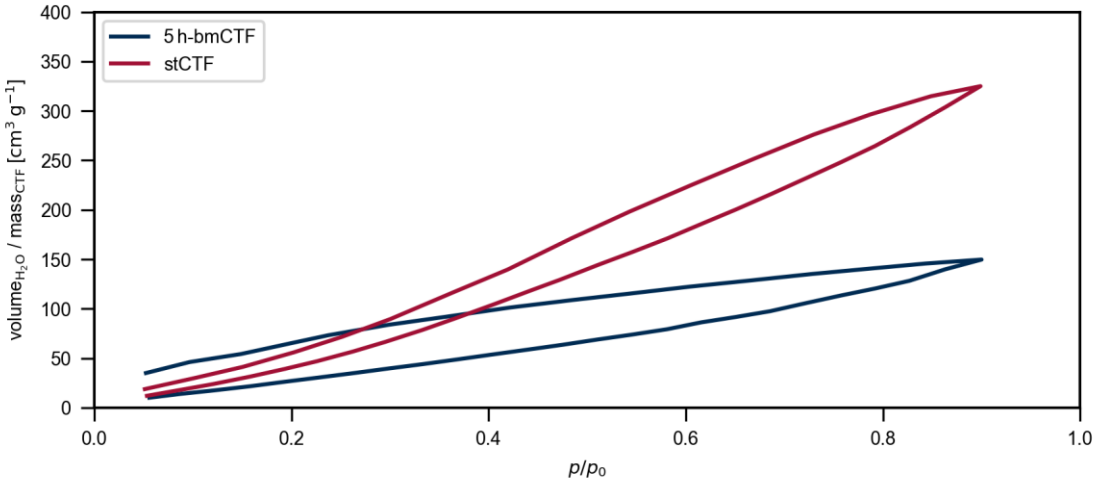

Figure S23. Water physisorption isotherms of stCTF (red) and bmCTF (dark blue) with volume of adsorbed water per CTF mass.

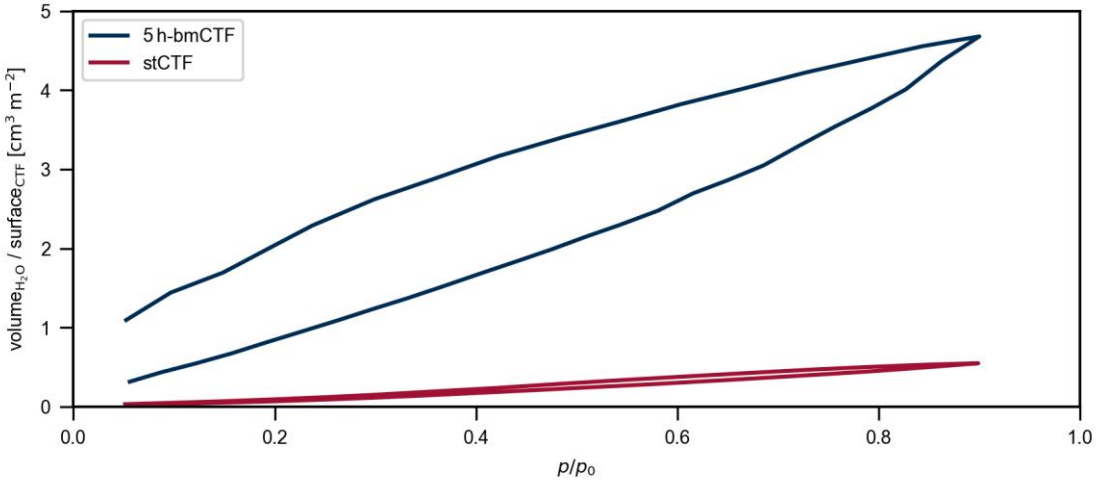

Figure S24. Water physisorption isotherms of stCTF (red) and bmCTF (dark blue) with volume of adsorbed water per m^2 of CTF surface.

S3.12. Thermogravimetric Analysis

Thermogravimetric analysis under air and nitrogen gas conditions was performed at a Netsch STA 449 F5 device by Jupiter. All measurements were performed by heating from 25 °C to minimum 750 °C at a heating rate of 5 K min^{-1}.

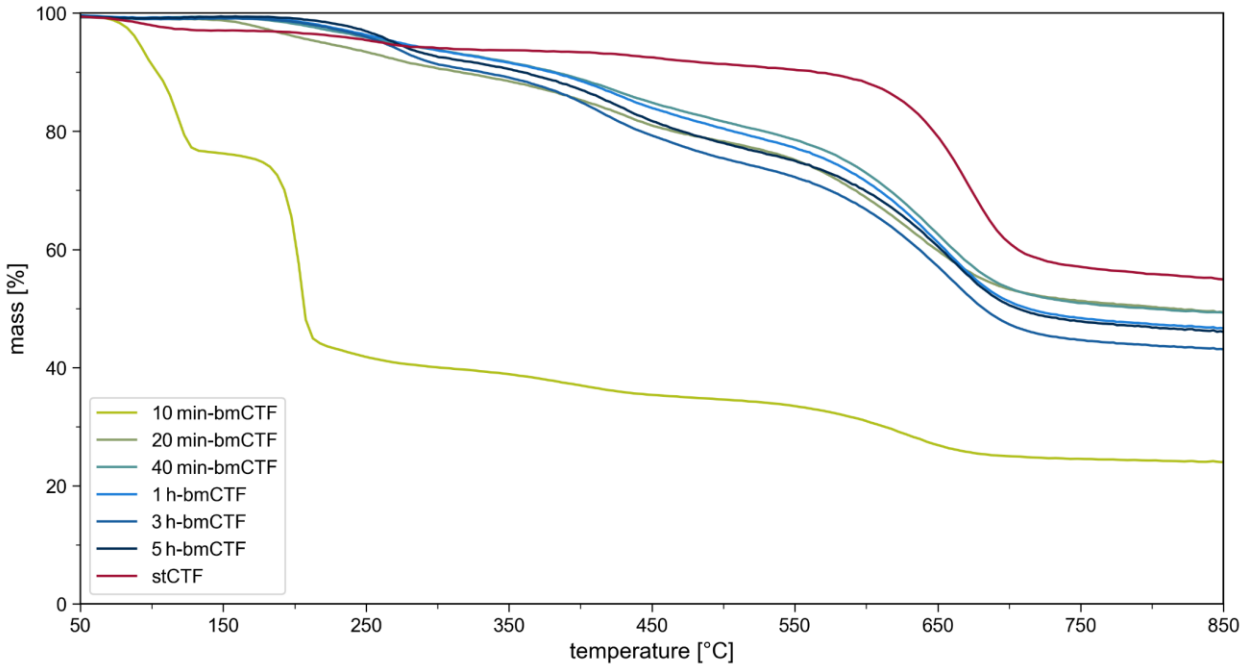

Figure S25. Thermogravimetric analysis for the stCTF (red), and bmCTFs at varying milling times of 10 min (pale green) to 5 h (dark blue) in N_2-atmosphere.

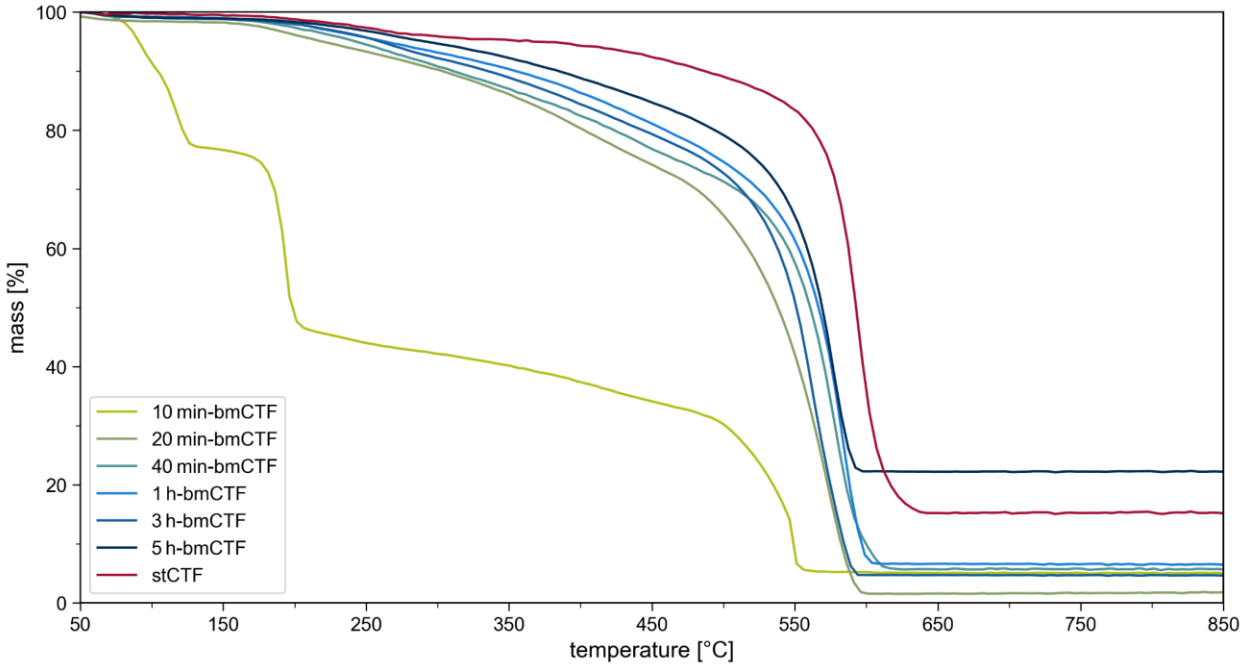

Figure S26. Thermogravimetric analysis for the stCTF (red), and bmCTFs at varying milling times of 10 min (pale green) to 5 h (dark blue) in air.

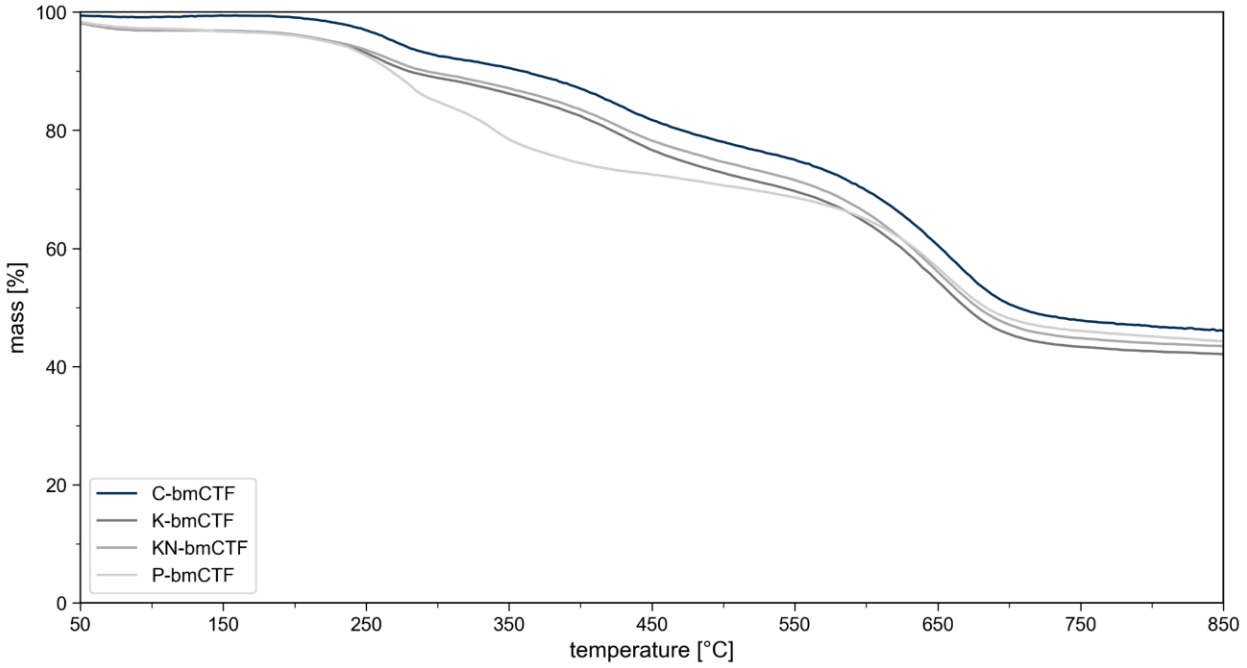

Figure S27. Thermogravimetric analysis for the C-bmCTF (blue), K-bmCTF (dark grey), KN-bmCTF (grey), and P-bmCTF (light grey) in N_2-atmosphere.

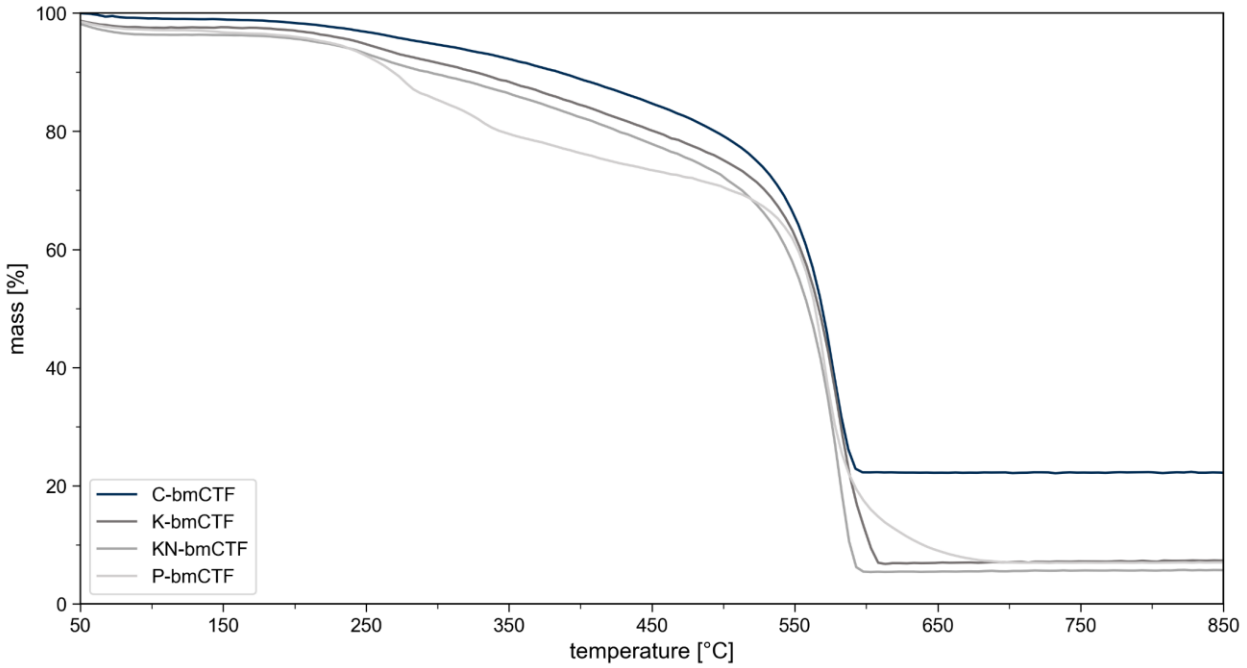

Figure S28. Thermogravimetric analysis for the C-bmCTF (blue), K-bmCTF (dark grey), KN-bmCTF (grey), and P-bmCTF (light grey) in air.

S3.13. SEM

Scanning electron microscopy (SEM) was conducted at a COMEX EM-30N benchtop SEM. Prior to measuring, all samples were sputtered with gold using a COMEX SPT-20 at 7 mA for 210 s. For this, the samples were placed on a carbon tape equipped sample holder.

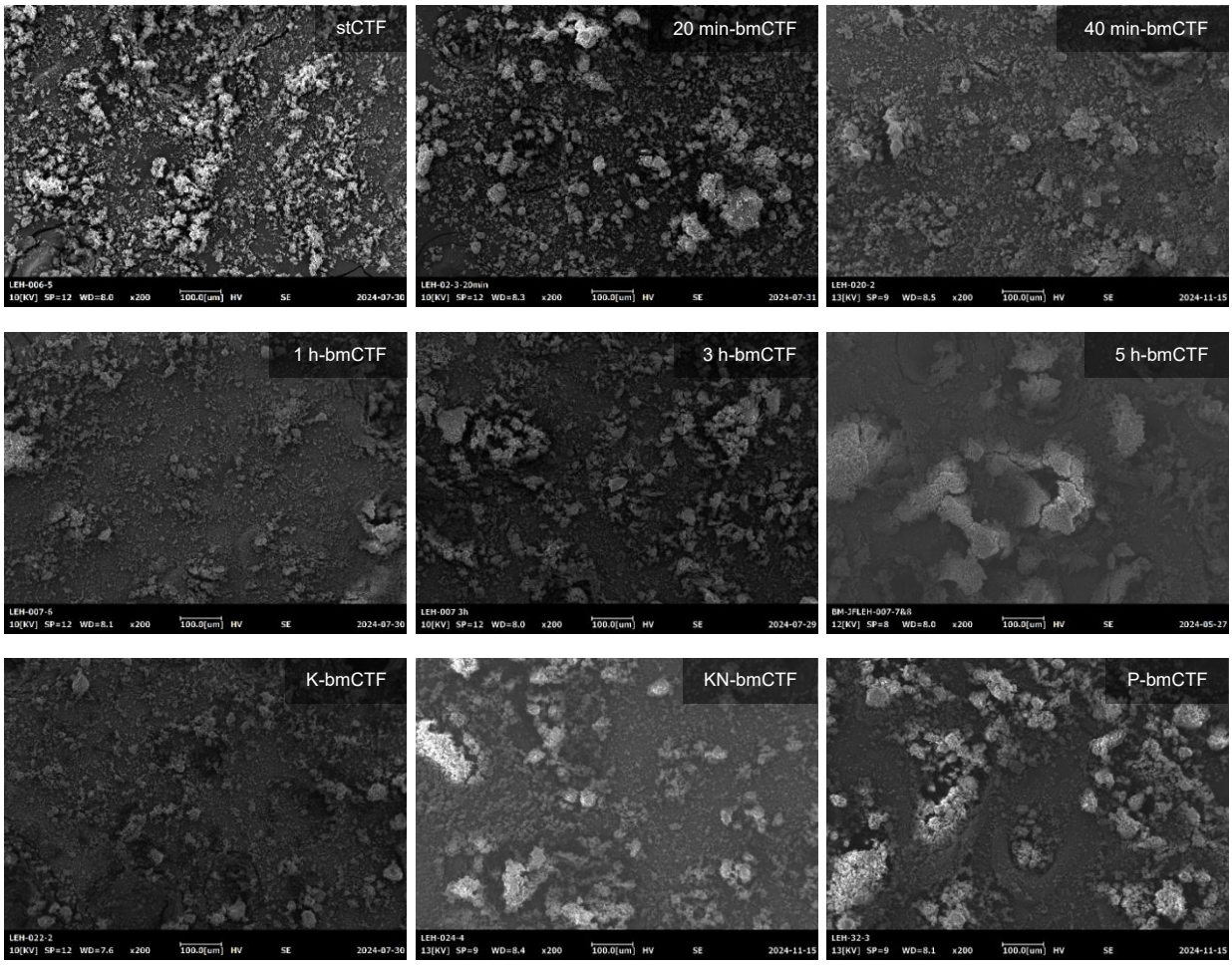

Figure S29. SEM pictures of the CTFs discussed in this work at a magnification of 200.

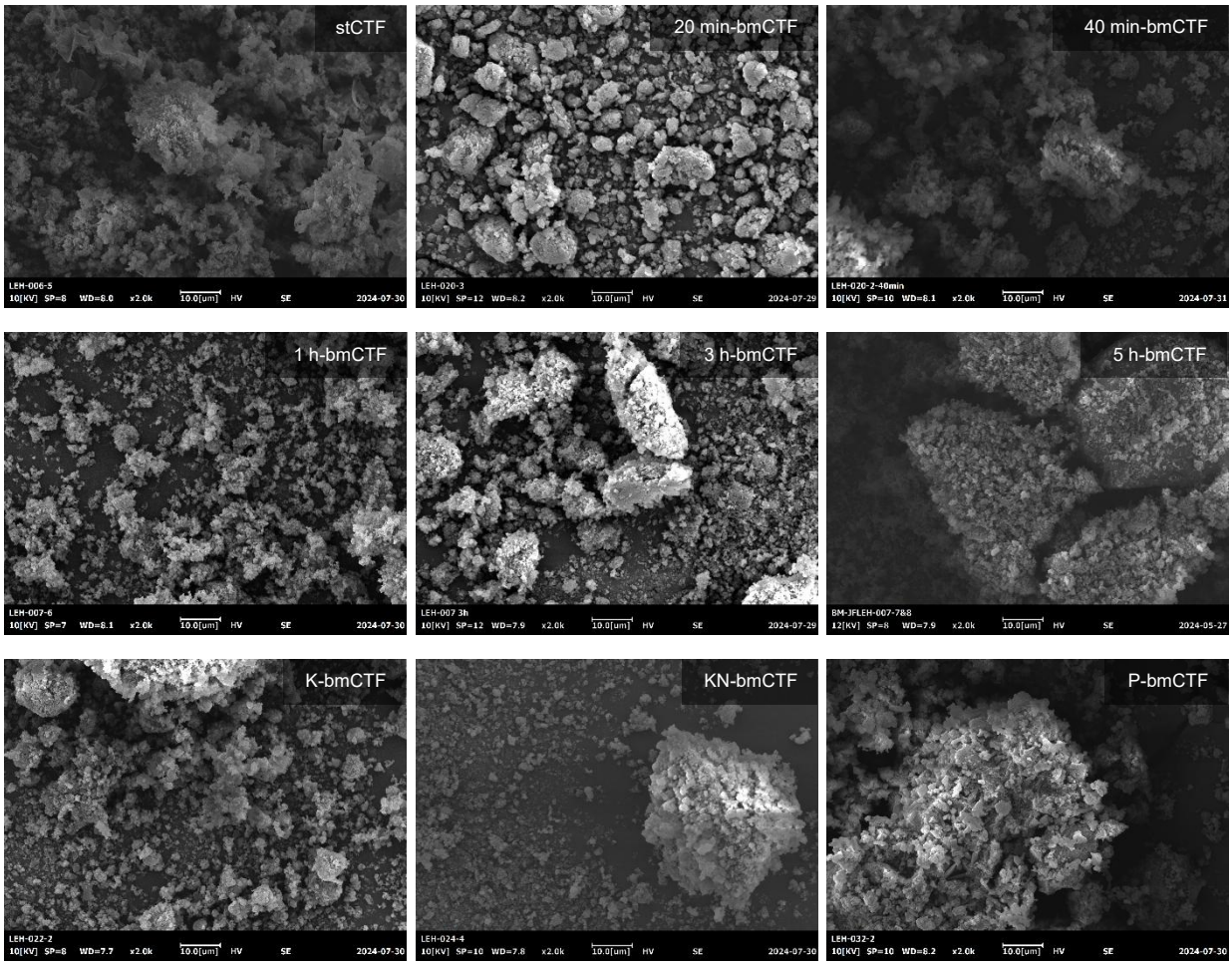

Figure S30. SEM pictures of the CTFs discussed in this work at a magnification of 2.0 k.

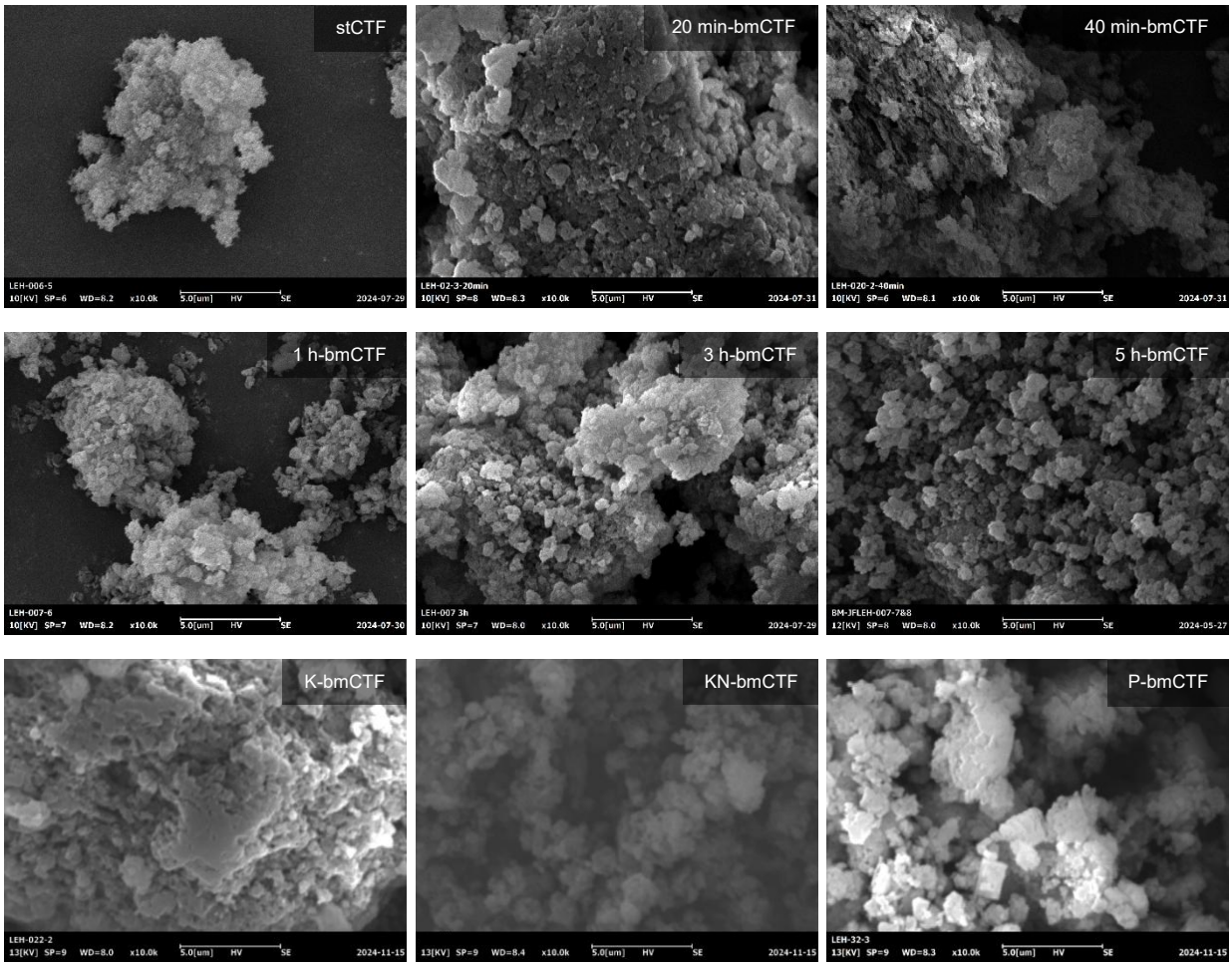

Figure S31. SEM pictures of the CTFs discussed in this work at a magnification of 10.0 k.

S3.14. UV-Vis Spectroscopy

Diffuse reflectance spectroscopy, as well as absorbance data, were measured using a UV-2600i UV Vis spectrometer by Shimadzu equipped with an Integrating Sphere Attachment and a two-detector-setup. All spectra were measured from 200 to 850 nm. As light sources, the standard halogen and deuterium lamps provided by Shimadzu were utilized, switching at 320 nm for the reflectance measurements and at 323 nm for the absorbance experiments, respectively. Prior to all measurements, a background using $BaSO_4$ was taken.

Table S6. Band gap energies and respective wavelengths calculated via the Tauc plot method for all materials discussed in this work.

Material	Band Gap Energy [eV]	Corresponding Wave Length [nm]
stCTF	3.08	403
10 min-bmCTF	2.78	446
20 min-bmCTF	2.66	466
40 min-bmCTF[a]	2.60 / 3.16	476 / 392
1 h-bmCTF[a]	2.56 / 3.13	484 / 396
3 h-bmCTF[a]	2.52 / 3.01	492 / 412
5 h-bmCTF / $bmCTF_2$ / C-bmCTF[a]	2.51 / 3.00	493 / 413
$bmCTF_1$[b]	2.48 / 2.88	500 / 430
$bmCTF_{1.5}$[b]	2.49 / 2.99	498 / 415
$bmCTF_3$[b]	2.48 / 2.87	499 / 432
stbmCTF[b]	2.40	517
K-bmCTF[a]	2.57 / 3.10	483 / 400
KN-bmCTF[a]	2.54 / 2.85	489 / 434
P-bmCTF[a]	2.43 / 2.89	510 / 428

[a] A second incline is detected for the bmCTFs with milling times of at least 40 min. Due to the major contribution of the first incline to the absorption of the materials, the smaller band gap energy is discussed for these materials.

[b] measured in the range of 300 to 800 nm.

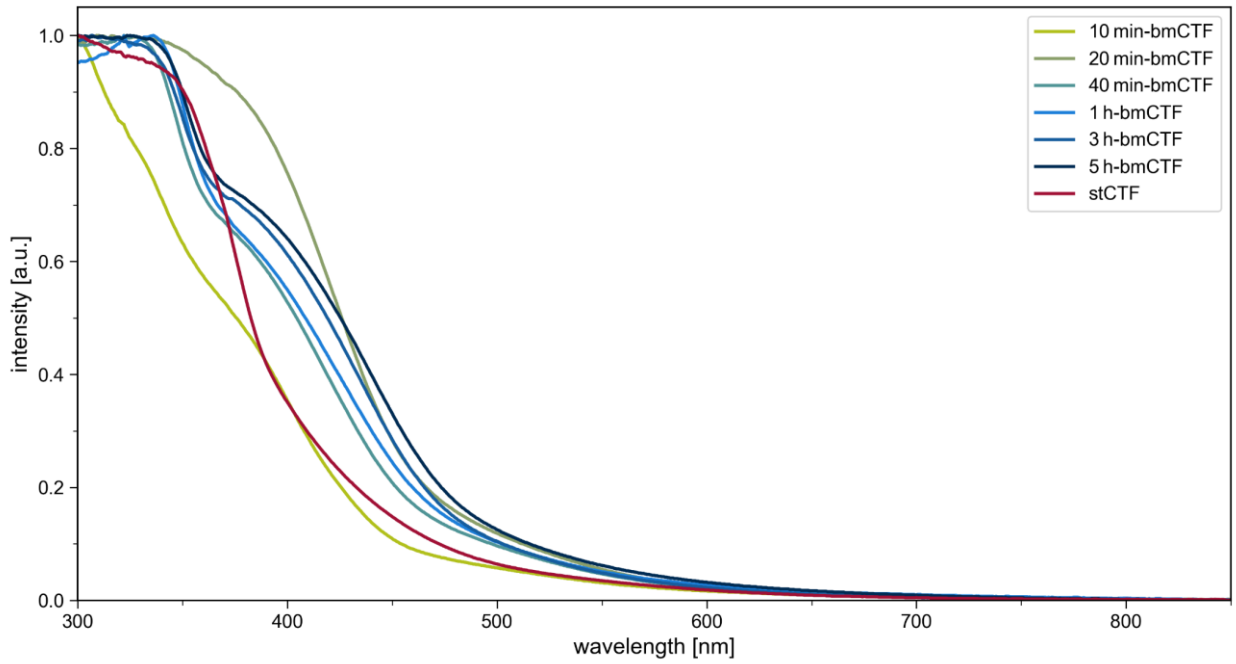

Figure S32. Absorption UV-Vis spectra for the stCTF (red), and bmCTFs at varying milling times of 10 min (pale green) to 5 h (dark blue).

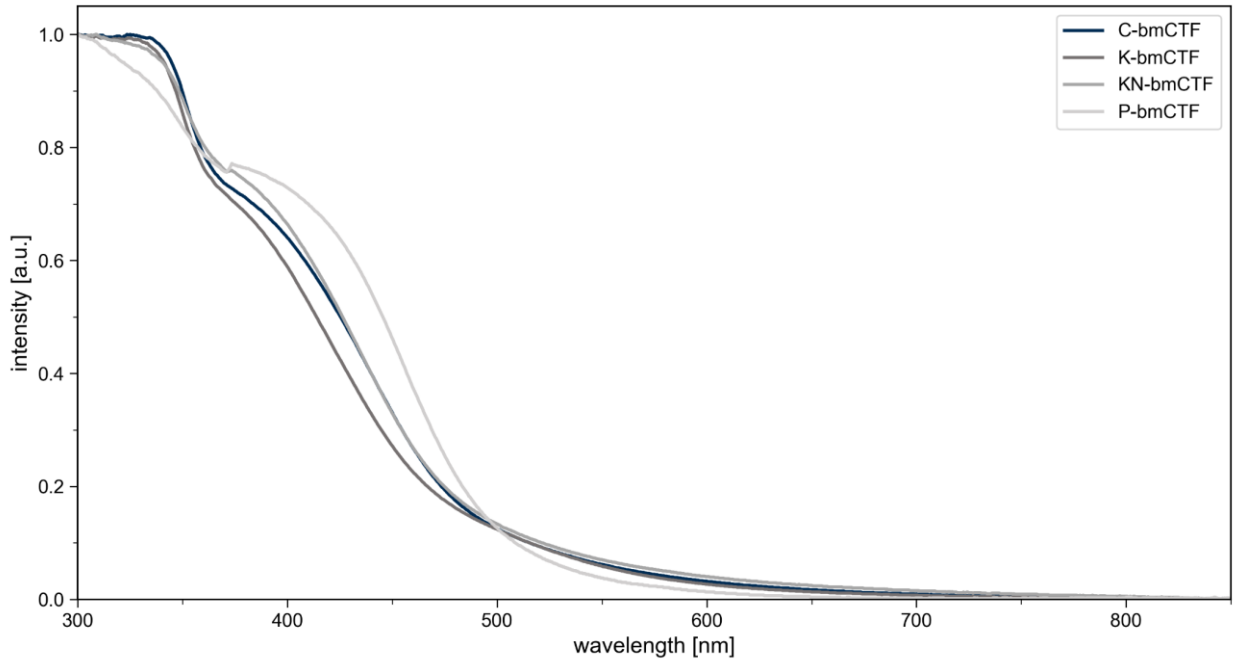

Figure S33. Absorption UV-Vis spectra for the for the C-bmCTF (blue), K-bmCTF (dark grey), KN-bmCTF (grey), and P-bmCTF (light grey).

S3.15. Photocatalytic Activities

White Light Experiments

All photocatalytic experiments were performed as a three-fold determination in an MPDS photoreactor setup by Peschl Ultraviolet GmbH using an 1000 W m^{-2} cool white LED. The experiments were conducted for 1 h at 25 °C, using 1.5 mg of catalyst in 6 mL of deionized water. A gas flow of synthetic air (50 mL min^{-1}) was applied via PTFE tubes to each reactor. For quantification of the final hydrogen peroxide concentration, samples were taken from the reaction solution and centrifuged for 5 min to remove remaining catalyst particles. The solution was then diluted with deionized water and mixed with the Spectroquant® test equipment by Merck (calibrated for 0.015 to 6.00 mg mL^{-1}) according to the manufacturer's specifications. All photometric measurements were performed at 450 nm in an UV-2600i UV Vis spectrometer by Shimadzu.

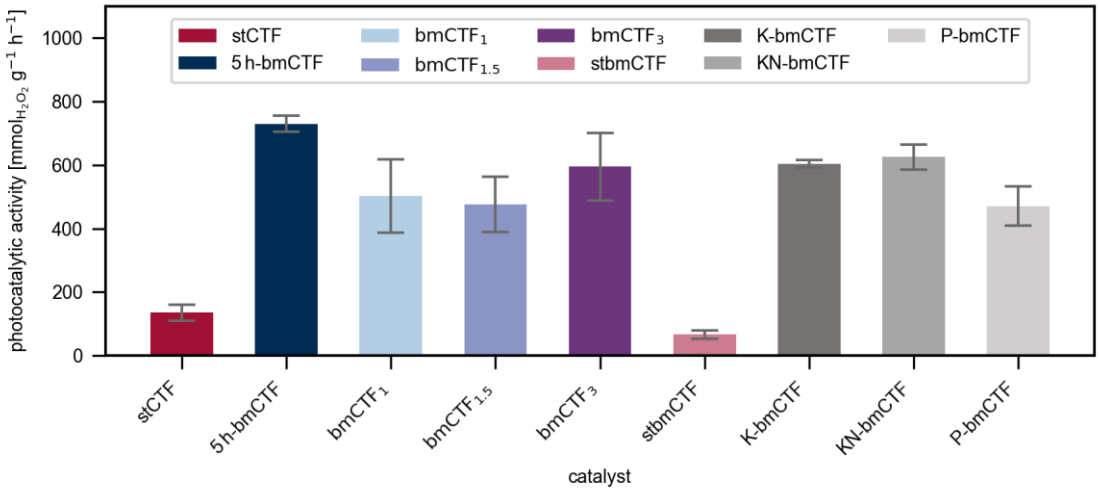

Figure S34. Photocatalytic activity of all CTF tested under cool white light irradiation.

Table S7. Photocatalytic activity of all CTFs tested under cool white light irradiation.

Catalyst	Photocatalytic Activity [µmol g^{-1} h^{-1}]
stCTF	135 ± 25
5 h-bmCTF / $bmCTF_2$ / C-bmCTF	730 ± 26
$bmCTF_1$	502 ± 116
$bmCTF_{1.5}$	476 ± 88
$bmCTF_3$	595 ± 106
stbmCTF	66 ± 14
K-bmCTF	604 ± 12
KN-bmCTF	625 ± 40
P-bmCTF	471 ± 62

Time-resolved Experiments

All photocatalytic experiments were performed as a two-fold determination on a PX9 photoreactor setup by Peschl Ultraviolet GmbH using a lamp palette equipped with nine cool-white LEDs. All lamps were run at 100 % equal irradiance modus (equivalent to 750 W m^{-2}). The experiments were performed at 25 °C, using 1.5 mg of catalyst in 6 mL of deionized water and applying shaking at 600 rpm. All reactions were started at the same time, while two reactors were removed from the setup after 30 min, 1 h, 2 h and 3 h each. Quantification of the final hydrogen peroxide concentration was performed as described for the white light experiments.

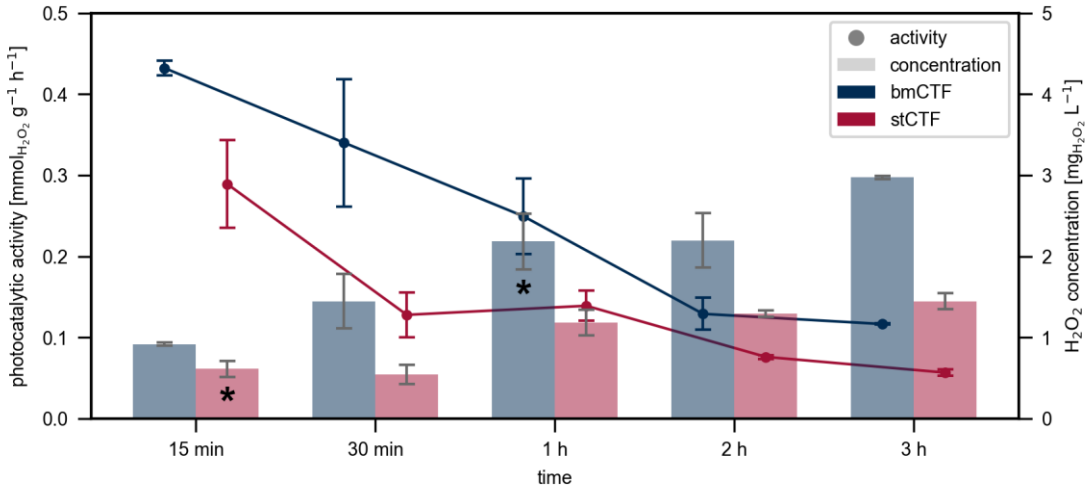

Figure S35. Photocatalytic activity and resulting hydrogen peroxide concentration of stCTF and 5 h-bmCTF at different irradiation times. Lines for the photocatalytic activity are added as a guide to the eye. (* separate run)

Table S8. Photocatalytic activity and resulting hydrogen peroxide concentration of stCTF and 5 h-bmCTF at different irradiation times

Irradiation Time	Photocatalytic Activity [µmol g^{-1} h^{-1}]		c(H_2O_2) [mg L^{-1}l]	
	stCTF	bmCTF	stCTF	bmCTF
15 min	290 ± 5	432 ± 9	0.61 ± 0.10	0.92 ± 0.02
30 min	128 ± 28	340 ± 79	0.54 ± 0.12	1.45 ± 0.33
1 h	139 ± 18	249 ± 47	1.18 ± 0.16	2.18 ± 0.35
2 h	76 ± 2	129 ± 20	1.29 ± 0.04	2.20 ± 0.33
3 h	57 ± 4	117 ± 1	1.45 ± 0.1	2.97 ± 0.02

Wavelength-resolved Experiments

All photocatalytic experiments were performed on a PX9 photoreactor setup by Peschl Ultraviolet GmbH using a lamp palette equipped with nine LEDs of different wavelengths. All lamps were run at 100 % equal irradiance modus (equivalent to 600 W m^{-2}). The experiments were performed for 1 h at 25 °C, using 3 mg of catalyst in 6 mL of deionized water and applying shaking at 600 rpm. Quantification of the final hydrogen peroxide concentration was performed as described for the white light experiments.

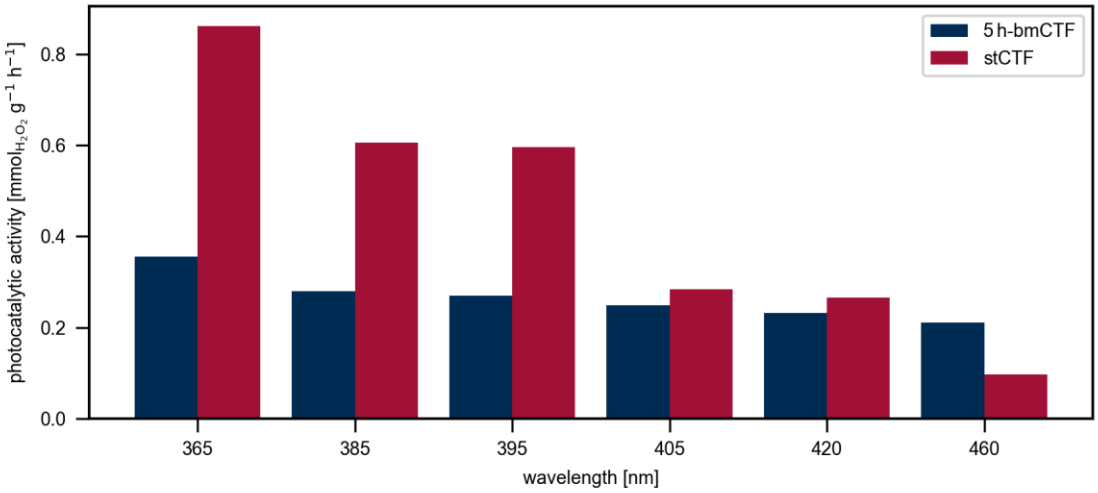

Figure S36. Photocatalytic activity of stCTF and 5 h-bmCTF at different wavelengths.

Table S9. Photocatalytic activity of the stCTF and 5 h-bmCTF at different wavelengths.

Wavelength [nm]	Photocatalytic Activity [µmol g^{-1} h^{-1}]	
	stCTF	5 h-bmCTF
365	862	355
385	605	280
395	596	270
405	283	248
420	266	232
460	96	211

Reference Experiments

Reference experiments, once without catalyst and once without irradiation with 1 mg of stCTF and 5 h-bmCTF were performed. Except for these modifications, the experiments were performed as three-fold determinations identically to the time-resolved experiments for a reaction time of 1 h. Quantification of the final hydrogen peroxide concentration was performed as described for the white light experiments.

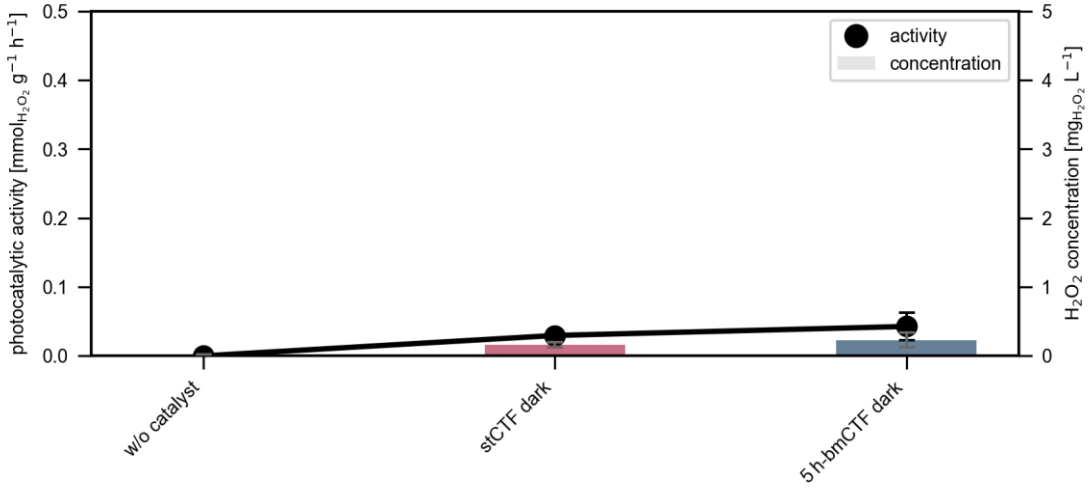

Figure S37. Photocatalytic activity for reference experiments without catalyst addition and without irradiation.

References

1 M. Liu, Q. Huang, S. Wang, Z. Li, B. Li, S. Jin and B. Tan, *Angew. Chem.*, 2018, **57**, 11968–11972.
2 D. Ditz, N. M. Sackers, F. Müller, M. Zobel, S. Bergwinkl, P. Nuernberger, L. S. Häser, S. Brettschneider, F. M. Wisser, C. Bannwarth and R. Palkovits, *Green Chem.*, 2024, **26**, 3397–3405.
3 N. Fantozzi, J.-N. Volle, A. Porcheddu, D. Virieux, F. García and E. Colacino, *Chem. Soc. Rev.*, 2023, **52**, 6680–6714.
4 S. Hediger, B. H. Meier and R. R. Ernst, *Chem. Phys. Lett.*, 1995, **240**, 449–456.
5 S. Hediger, B. H. Meier, N. D. Kurur, G. Bodenhausen and R. R. Ernst, *Chem. Phys. Lett.*, 1994, **223**, 283–288.
6 J. Filik, A. W. Ashton, P. C. Y. Chang, P. A. Chater, S. J. Day, M. Drakopoulos, M. W. Gerring, M. L. Hart, O. V. Magdysyuk, S. Michalik, A. Smith, C. C. Tang, N. J. Terrill, M. T. Wharmby and H. Wilhelm, *J. Appl. Crystallogr.*, 2017, **50**, 959–966.
7 T. Egami and S. J. Billinge, *Underneath the Bragg peaks : structural analysis of complex materials*, Pergamon, Amsterdam, 2nd edn., 2012.
8 S. J. L. Billinge, in *International Tables for Crystallography*, 2019, vol. H, pp. 649–672.
9 P. Juhás, T. Davis, C. L. Farrow and S. J. L. Billinge, *J. Appl. Crystallogr.*, 2013, **46**, 560–566.